An analysis of finite element approximation in electrical impedance tomography

2014 Inverse Problems 30 045013

(http://iopscience.iop.org/0266-5611/30/4/045013)

IOP Publishing Inverse Problems

Inverse Problems **30** (2014) 045013 (24pp) doi:10.1088/0266-5611/30/4/045013

An analysis of finite element approximation in electrical impedance tomography

Matthias Gehre[1], **Bangti Jin**[2] **and Xiliang Lu**[3]

[1] Center for Industrial Mathematics, University of Bremen, Bremen D-28359, Germany
[2] Department of Mathematics, University of California, Riverside, 900 University Ave, Riverside, CA 92521, USA
[3] School of Mathematics and Statistics, Wuhan University, Wuhan 430072, People's Republic of China

E-mail: mgehre@math.uni-bremen.de, bangti.jin@gmail.com and xllv.math@whu.edu.cn

Received 5 December 2013, revised 3 February 2014
Accepted for publication 13 February 2014
Published 18 March 2014

Abstract

We present a finite element analysis of electrical impedance tomography for reconstructing the conductivity distribution from electrode voltage measurements by means of Tikhonov regularization. Two popular choices of the penalty term, i.e., the $H^1(\Omega)$-norm smoothness penalty and total variation seminorm penalty, are considered. A piecewise linear finite element method is employed for discretizing the forward model, i.e., the complete electrode model, the conductivity, and the penalty functional. The convergence of the finite element approximations for the Tikhonov model on both polyhedral and smooth curved domains is established. This provides rigorous justifications for the ad hoc discretization procedures. Numerical experiments confirm the convergence analysis.

Keywords: electrical impedance tomography, finite element approximation, convergence analysis, Tikhonov regularization

(Some figures may appear in colour only in the online journal)

1. Introduction

Electrical impedance tomography (EIT) is a very popular diffusive imaging modality for probing internal structures of the concerned object, by recovering its electrical conductivity/permittivity distribution from voltage measurements on the boundary. One typical experimental setup is as follows. One first attaches a set of metallic electrodes to the surface of the object. Then one injects an electric current into the object through these electrodes,

which induces an electromagnetic field inside the object. Finally, one measures the electric voltages on these electrodes. The procedure is often repeated several times with different input currents in order to yield sufficient information on the sought-for conductivity distribution. This physical process can be most accurately described by the complete electrode model (CEM) [8, 35], but the simpler continuum model is also frequently employed in simulation studies. The imaging modality has attracted considerable interest in applications, e.g., in medical imaging, geophysical prospecting, nondestructive evaluation and pneumatic oil pipeline conveying.

Due to its broad range of prospective applications, a large number of imaging algorithms have been developed, and have delivered very encouraging reconstructions. These methods essentially utilize the idea of regularization in diverse forms, in order to overcome the severe ill-posed nature of the imaging task, and occasionally also the idea of (recursive) linearization to enable computational tractability. We refer interested readers to the reviews [1, 4] and references [9, 20, 21, 24, 26, 28, 30, 33, 34] for a very incomplete list of existing imaging methods. One prominent idea underlying many popular EIT imaging techniques is Tikhonov regularization with convex variational penalties, e.g., smoothness, total variation and more recently sparsity constraints [21, 23]. These approaches have demonstrated very promising reconstructions for real data [5, 18, 25]. However, the analysis of such Tikhonov formulations, surprisingly, has not received due attention, despite their popularity in and relevance to practical applications. We are only aware of very few works in this direction [22, 32, 33]. In the interesting works [32, 33], Rondi and Santosa analyzed the existence, stability and consistency of the Mumford–Shah/total variation formulation. Recently, Jin and Maass [22] established the existence, stability, consistency and especially convergence rates for the conventional Sobolev H^1-penalty and sparsity constraints. These works provide partial theoretical justifications for the practical usage of related imaging algorithms.

In practice, the numerical implementation of these imaging algorithms inevitably requires discretizing the forward model and the Tikhonov functional into a finite-dimensional discrete problem. This is often achieved by the finite element method, due to its versatility for handling general domain geometries, spatially varying coefficients and solid theoretical underpinnings. However, the solution to the discrete optimization problem is different from that to the continuous Tikhonov model due to the discretization errors. This raises several interesting questions on the discrete approximations. One fundamental question is about the validity of the discretization procedure: does the discrete approximation converge to a solution to the continuous Tikhonov formulation as the mesh size tends to zero? Since for inverse problems, small errors in the data/model can possibly cause large deviations in the solution, it is unclear whether the discretization error induces only small changes on the solution. Hence, the validity of the discretization strategy does not follow automatically. To the best of our knowledge, the convergence issue has not been addressed for Tikhonov regularization of EIT, despite its routine applications.

However, there are several related works [14, 27, 28]. In the interesting work [14], Ervedoza and de Gournay obtained a stability estimate for the discrete Calderon problem (uniform with respect to the discretization parameter h), by using discrete Carleman estimates for the discrete Laplace operator. The work focuses on the discrete Dirichlet-to-Neumann map. In [29], Lechleiter and Rieder established the convergence of the finite element discretization of the EIT forward problem, for the special case of piecewise polynomial conductivity fields. However, the conductivity fields are not discretized in the convergence analysis. Further, we note also that a closely related problem of compensating the effect of an imprecise boundary on the resolution of numerical reconstructions has been studied in [27].

In this work, we address the convergence issue of finite element approximations. Specifically, we consider the CEM, and discuss two popular imaging techniques based on

Tikhonov regularization with smoothness/total variation penalties. These methods have been extensively used [5, 9, 12, 33, 36, 37]. We shall distinguish two different scenarios: polyhedral domains and convex smooth curved domains. The former allows exact triangulation with simplicial elements, whereas the latter invokes domain approximations and hence the analysis is much more involved. The simpler polyhedral case serves to illustrate the main ideas of the proof. We remark that for practical applications, curved domains are very common and their accurate discrete description is essential for getting reasonable reconstructions, e.g., in imaging human body, and hence it is of immense interest to analyze this case.

The rest of the paper is organized as follows. In section 2, we describe the CEM, collect some preliminary regularity results, and recall the Tikhonov regularization formulation. Then the convergence analysis for polyhedral domains is discussed in section 3, and for curved domains in section 4. In section 5, two numerical examples are presented to illustrate the convergence theory. Finally, concluding remarks are given in section 6. Throughout, we shall use C to denote a generic constant, which may differ at different occurrences but does not depend on the mesh size h. We shall also use standard notation from [15] for the Sobolev spaces $W^{m,p}(\Omega)$.

2. Preliminaries

Here we recapitulate the mathematical formulation of the CEM and discuss its analytical properties. We shall also briefly describe the continuous Tikhonov formulation.

2.1. Complete electrode model

According to the comparative experimental studies in [8, 35], the CEM is currently the most accurate mathematical model for reproducing EIT experimental data. This is attributed to its faithful modeling of the physics: it takes into account several important features of real EIT experiments, i.e., discrete nature of the electrodes, shunting effect and contact impedance effect. We shall briefly describe the mathematical model and its analytical properties in this part. These properties will be useful in the convergence analysis below.

Let Ω be an open and bounded domain in $\mathbb{R}^d$ ($d = 2, 3$) with a Lipschitz continuous boundary Γ. We denote the set of electrodes by $\{e_l\}_{l=1}^L$, which are open connected subsets of the boundary Γ and disjoint from each other, i.e., $\bar{e}_i \cap \bar{e}_k = \emptyset$ if $i \neq k$. The applied current on the lth electrode e_l is denoted by I_l, and the current vector $I = (I_1, \ldots, I_L)^t$ satisfies $\sum_{l=1}^L I_l = 0$ in view of the law of charge conservation. Let the space $\mathbb{R}_\diamond^L$ be the subspace of the vector space $\mathbb{R}^L$ with zero mean, then we have $I \in \mathbb{R}_\diamond^L$. The electrode voltage $U = (U_1, \ldots, U_L)^t$ is normalized such that $U \in \mathbb{R}_\diamond^L$, which represents a grounding condition. Then the mathematical model for the CEM reads: given the electrical conductivity σ, positive contact impedances $\{z_l\}_{l=1}^L$ and an input current pattern $I \in \mathbb{R}_\diamond^L$, find the potential $u \in H^1(\Omega)$ and electrode voltage $U \in \mathbb{R}_\diamond^L$ such that

$$\begin{cases} -\nabla \cdot (\sigma \nabla u) = 0 & \text{in } \Omega, \\ u + z_l \sigma \dfrac{\partial u}{\partial n} = U_l & \text{on } e_l, l = 1, 2, \ldots, L, \\ \displaystyle\int_{e_l} \sigma \frac{\partial u}{\partial n} \mathrm{d}s = I_l & \text{for } l = 1, 2, \ldots, L, \\ \sigma \dfrac{\partial u}{\partial n} = 0 & \text{on } \Gamma \setminus \cup_{l=1}^L e_l. \end{cases} \tag{1}$$

The physical motivation behind the model (1) is as follows. The governing equation is derived under a quasi-static low frequency assumption on the electromagnetic process [35]. The second line describes the contact impedance effect: when injecting electrical currents into the object, a highly resistive thin layer forms at the electrode–electrolyte interface (due to certain electrochemical processes), which causes potential drops across the electrode–electrolyte interface. The potential drop is described by Ohm's law. Further, it takes into account the fact that metallic electrodes are perfect conductors, and hence the voltage is constant on each electrode. The third line reflects the fact that the current I_l injected through the electrode e_l is completely confined to e_l. The complex boundary conditions faithfully capture the physical process, and thus the model (1) is capable of reproducing experimental data within the measurement precision [8, 35].

Due to physical constraint, the conductivity distribution is naturally bounded both from below and from above by positive constants, hence we introduce the following admissible set

$$\mathcal{A} = \{\sigma : \lambda \leqslant \sigma(x) \leqslant \lambda^{-1} \text{ a.e. } x \in \Omega\},$$

for some $\lambda \in (0, 1)$. We shall endow the set with $L^r(\Omega)$ norms, $r \geqslant 1$.

We denote by $\mathbb{H}$ the product space $H^1(\Omega) \otimes \mathbb{R}^L_\diamond$ with its norm defined by

$$\|(u, U)\|^2_{\mathbb{H}} = \|u\|^2_{H^1(\Omega)} + \|U\|^2_{\mathbb{R}^L}.$$

A convenient equivalent norm on the space $\mathbb{H}$ is given in the next lemma [35].

Lemma 2.1. *On the space $\mathbb{H}$, the norm $\|\cdot\|_{\mathbb{H}}$ is equivalent to the norm $\|\cdot\|_{\mathbb{H},*}$ defined by*

$$\|(u, U)\|^2_{\mathbb{H},*} = \|\nabla u\|^2_{L^2(\Omega)} + \sum_{l=1}^{L} \|u - U_l\|^2_{L^2(e_l)}.$$

The weak formulation of the model (1) reads: find $(u, U) \in \mathbb{H}$ such that

$$\int_\Omega \sigma \nabla u \cdot \nabla v \, \mathrm{d}x + \sum_{l=1}^{L} z_l^{-1} \int_{e_l} (u - U_l)(v - V_l) \, \mathrm{d}s = \sum_{l=1}^{L} I_l V_l \quad \forall (v, V) \in \mathbb{H}. \tag{2}$$

Now for any fixed $\sigma \in \mathcal{A}$, the existence and uniqueness of a solution $(u, U) \equiv (u(\sigma), U(\sigma)) \in \mathbb{H}$ to the weak formulation (2) follows directly from lemma 2.1 and Lax–Milgram theorem, and further, it depends continuously on the input current pattern I [35]. The next result presents an improved regularity of the solution $(u(\sigma), U(\sigma))$ to system (1). It can be derived from the Neumann analogue [17, 19] of Meyers' celebrated gradient estimates [31]; see [22] for details.

Theorem 2.1. *Let $\lambda \in (0, 1)$, and $\sigma(x) \in [\lambda, \lambda^{-1}]$ almost everywhere. Then there exists a constant $Q(\lambda, d) > 2$, which depends only on the domain Ω, the spatial dimension d and the constant λ, such that for any $q \in (2, Q(\lambda, d))$, the solution $(u(\sigma), U(\sigma)) \in \mathbb{H}$ to system (1) satisfies the following estimate*

$$\|u\|_{W^{1,q}(\Omega)} \leqslant C\|I\|,$$

where the constant $C = C(\Omega, d, \lambda, q)$.

Remark 2.1. The parameter Q depends on the regularity of the domain Ω. If the domain Ω is of class C^1, then $Q(\lambda, d) \to \infty$ as $\lambda \to 1$ [19]. For a general Lipschitz domain, e.g., polyhedrons, there also always exists some $Q(\lambda, d) > 2$ for any $\lambda < 1$, cf [19, section 5].

The next result shows that the parameter-to-state map $\sigma \to (u(\sigma), U(\sigma)) \in \mathbb{H}$ is continuous with respect to the $L^r(\Omega)$ topology on the admissible set $\mathcal{A}$.

Lemma 2.2. *Let the sequence $\{\sigma_n\} \subset \mathcal{A}$ converge to some $\sigma^* \in \mathcal{A}$ in $L^r(\Omega)$, $r \geqslant 1$. Then the sequence of the solutions $\{(u(\sigma_n), U(\sigma_n))\}$ converges to $(u(\sigma^*), U(\sigma^*))$ in $\mathbb{H}$.*

Proof. It follows from the weak formulations of the solutions $(u_n, U_n) \equiv (u(\sigma_n), U(\sigma_n))$ and $(u^*, U^*) \equiv (u(\sigma^*), U(\sigma^*))$ (cf (2)) that for all $(v, V) \in \mathbb{H}$

$$\int_\Omega \sigma_n \nabla(u^* - u_n) \cdot \nabla v \, \mathrm{d}x + \int_\Omega (\sigma^* - \sigma_n) \nabla u^* \cdot \nabla v \, \mathrm{d}x + \sum_{l=1}^{L} z_l^{-1} \int_{e_l} (u^* - u_n - U_l^* + U_{n,l})(v - V_l) \, \mathrm{d}s = 0.$$

Upon setting the test function (v, V) to $(u^* - u_n, U^* - U_n) \in \mathbb{H}$ in this identity, and using theorem 2.1 and the generalized Hölder's inequality, we derive

$$\begin{aligned}
\min\left(\lambda, \{z_l^{-1}\}\right) &\left(\|\nabla(u^* - u_n)\|_{L^2(\Omega)}^2 + \sum_{l=1}^{L} \|u^* - u_n - U_l^* + U_{n,l}\|_{L^2(e_l)}^2 \right) \\
&\leqslant \int_\Omega \sigma_n |\nabla(u^* - u_n)|^2 \, \mathrm{d}x + \sum_{l=1}^{L} z_l^{-1} \int_{e_l} |u^* - u_n - U_l^* + U_{n,l}|^2 \, \mathrm{d}s \\
&= -\int_\Omega (\sigma^* - \sigma_n) \nabla u^* \cdot \nabla(u^* - u_n) \, \mathrm{d}x \\
&\leqslant \|\sigma^* - \sigma_n\|_{L^p(\Omega)} \|\nabla u^*\|_{L^q(\Omega)} \|\nabla(u^* - u_n)\|_{L^2(\Omega)} \\
&\leqslant \|\sigma^* - \sigma_n\|_{L^p(\Omega)} \|\nabla u^*\|_{L^q(\Omega)} \|(u^* - u_n, U^* - U_n)\|_{\mathbb{H}},
\end{aligned}$$

where the exponent $q \in (2, Q(\lambda, d))$ is from theorem 2.1 and the exponent p satisfies $p^{-1} + q^{-1} = 2^{-1}$. The desired assertion follows immediately if $r \geqslant p$. In the case $r < p$, we exploit the $L^\infty(\Omega)$ bound of the admissible set $\mathcal{A}$, i.e.,

$$\int_\Omega |\sigma^* - \sigma_n|^p \, \mathrm{d}x \leqslant \lambda^{r-p} \int_\Omega |\sigma^* - \sigma_n|^r \, \mathrm{d}x.$$

This together with lemma 2.1 shows the desired assertion. □

2.2. Tikhonov regularization

The EIT inverse problem is to reconstruct an approximation to the physical conductivity $\sigma^\dagger$ from noisy measurements U^δ of the electrode voltage $U(\sigma^\dagger)$, corresponding to several input currents. It is severely ill-posed in the sense that small errors in the data can lead to very large deviations in the solutions. Therefore, some sort of regularization is beneficial, and it is usually incorporated into EIT imaging algorithms, either implicitly or explicitly, in order to yield stable yet accurate conductivity images. One of the most popular and successful techniques is the standard Tikhonov regularization. It amounts to minimizing the celebrated Tikhonov functional

$$\min_{\sigma \in \mathcal{A}} \left\{ J(\sigma) = \tfrac{1}{2} \|U(\sigma) - U^\delta\|^2 + \alpha \Psi(\sigma) \right\}, \tag{3}$$

and then taking the minimizer, denoted by σ_α^δ, as an approximation to the sought-for physical conductivity $\sigma^\dagger$. Here the first term in the functional J captures the information encapsulated in the data U^δ. For simplicity, we consider only one dataset, and the adaptation to multiple

datasets is straightforward. The scalar $\alpha > 0$ is known as a regularization parameter, and controls the tradeoff between the two terms. The second term $\Psi(\sigma)$ in the functional J imposes *a priori* regularity knowledge (smoothness) on the expected conductivity distributions. Two most commonly used penalties are $\Psi(\sigma) = \frac{1}{2}\|\sigma\|^2_{H^1(\Omega)}$ and $\Psi(\sigma) = |\sigma|_{\mathrm{TV}(\Omega)}$ in the space of functions with bounded variation, i.e.,

$$\mathrm{BV}(\Omega) = \{v \in L^1(\Omega) : \|v\|_{\mathrm{BV}(\Omega)} < \infty\},$$

where $\|v\|_{\mathrm{BV}(\Omega)} = \|v\|_{L^1(\Omega)} + |v|_{\mathrm{TV}(\Omega)}$ with the total variation semi-norm $|v|_{\mathrm{TV}(\Omega)} = \int_\Omega |Dv|$ defined by

$$\int_\Omega |Dv| = \sup_{\substack{g\in(C_0^1(\Omega))^d \\ |g(x)|\leqslant 1}} \int_\Omega v \,\mathrm{div}(g)\,\mathrm{d}x.$$

Here the $H^1(\Omega)$-smoothness approach allows reconstructing conductivity distributions that are globally smooth, which often retains well their main features, whereas the total variation approach is well suited to discontinuous, especially piecewise constant, conductivity distributions [9, 33]. These two approaches represent the most popular EIT imaging techniques in practice. Theoretically, the existence and consistency of the continuous model (3) for the total variation and smoothness penalty have recently been established in [32] and [22], respectively, where in the latter work convergence rates for the smoothness and sparsity constraints were also provided.

One useful tool in the convergence analysis is the following embedding results [2, 15].

Lemma 2.3. *The spaces* $H^1(\Omega)$ *and* $\mathrm{BV}(\Omega)$ *have the following embedding properties:*

(a) The space $H^1(\Omega)$ *embeds compactly into* $L^p(\Omega)$ *for* $p < \infty$ *if* $d = 2$ *and* $p < 6$ *if* $d = 3$.
(b) The space $\mathrm{BV}(\Omega)$ *embeds compactly into* $L^p(\Omega)$ *for* $p < \frac{d}{d-1}$.

A direct consequence of lemmas 2.2 and 2.3 is the weak continuity. The concept of weak convergence in the BV space used below follows [2, definition 10.1.2].

Corollary 2.1. *Let the sequence* $\{\sigma_n\} \subset \mathcal{A}$ *converge to some* $\sigma^* \in \mathcal{A}$ *weakly in either* $H^1(\Omega)$ *or* $\mathrm{BV}(\Omega)$. *Then the sequence of the solutions* $\{(u(\sigma_n), U(\sigma_n))\}$ *converges strongly to* $(u(\sigma^*), U(\sigma^*))$ *in* $\mathbb{H}$.

Corollary 2.1 implies that the forward parameter-to-state map is weakly sequentially closed, and in view of the classical nonlinear Tikhonov regularization theory [13], this directly yields the existence of a minimizer and its stability. We will also need the following density result for the space $\mathrm{BV}(\Omega)$; see [7, lemma 3.3] for a proof.

Lemma 2.4. *Let* $g \in \mathrm{BV}(\Omega)$. *Then for any* $\epsilon > 0$, *there exists a function* $g_\epsilon \in C^\infty(\overline{\Omega})$ *such that*

$$\int_\Omega |g - g_\epsilon|\,\mathrm{d}x < \epsilon, \quad \left|\int_\Omega |\nabla g_\epsilon|\,\mathrm{d}x - \int_\Omega |Dg|\right| < \epsilon.$$

In order to obtain conductivity images from a computer implementation of the Tiknonov approach, one necessarily needs to discretize the forward problem (1) and the Tikhonov functional (3) by restricting the admissible conductivities to a certain finite-dimensional subspace. In practice, this is usually achieved by the finite element method due to its solid theoretical foundation and versatility for handling general domain geometries, as often occurs in practical scenarios. The main goal of the present study is to provide theoretical justifications for such procedures. We shall discuss two scenarios separately: polyhedral domains and (convex) smooth curved domains in sections 3 and 4, respectively.

3. Convergence for polyhedral domains

In this part, we discuss the case of polyhedral domains. Let Ω be an open bounded polyhedral domain. To discretize the imaging problem, we first triangulate the domain Ω. Let $\mathcal{T}_h$ be a family of shape regular, quasi-uniform triangulation of the domain Ω, with the mesh consisting of simplicial elements. The mesh size (the radius of the smallest circle/sphere circumscribing largest element) of the mesh $\mathcal{T}_h$ is denoted by h. On the mesh $\mathcal{T}_h$, we define a continuous piecewise linear finite element space

$$V_h = \{v \in C(\overline{\Omega}) : v|_T \in P_1(T)\ \forall T \in \mathcal{T}_h\},$$

where the space $P_1(T)$ consists of all linear functions on the element T. The same space V_h is used for approximating both the potential u and the conductivity σ. Nonetheless, we observe that in practice, it is possible to employ different meshes for the potential and the conductivity, for which the analysis below remains valid upon minor modifications. The use of piecewise linear finite elements is especially popular since the data (conductivity and boundary conditions) has only limited regularity.

With the space V_h, we can define two important operators: the canonical nodal interpolation operator $\mathcal{I}_h : C(\overline{\Omega}) \to V_h$ and the H^1-projection operator $\mathcal{R}_h : H^1(\Omega) \to V_h$ defined by

$$\int_\Omega \nabla \mathcal{R}_h u \cdot \nabla v \,\mathrm{d}x + \int_\Omega \mathcal{R}_h u v \,\mathrm{d}x = \int_\Omega \nabla u \cdot \nabla v \,\mathrm{d}x + \int_\Omega uv \,\mathrm{d}x \quad \forall v \in V_h.$$

It is well known [10] that the operators $\mathcal{I}_h$ and $\mathcal{R}_h$ satisfy for any $p > d$

$$\begin{aligned} &\lim_{h\to 0} \|v - \mathcal{I}_h v\|_{L^\infty(\Omega)} = 0 \quad \forall v \in W^{1,p}(\Omega), \\ &\lim_{h\to 0} \|v - \mathcal{R}_h v\|_{H^1(\Omega)} = 0 \quad \forall v \in H^1(\Omega). \end{aligned} \tag{4}$$

Now we can describe the finite element approximation scheme. First, we approximate the forward map $(u(\sigma), U(\sigma)) \in \mathbb{H}$ by $(u_h, U_h) \equiv (u_h(\sigma_h), U_h(\sigma_h)) \in \mathbb{H}_h \equiv V_h \otimes \mathbb{R}^L_\diamond$ defined by

$$\int_\Omega \sigma_h \nabla u_h \cdot \nabla v_h \,\mathrm{d}x + \sum_{l=1}^L z_l^{-1} \int_{e_l} (u_h - U_{h,l})(v_h - V_l) \,\mathrm{d}s = \sum_{l=1}^L I_l V_l \quad \forall (v_h, V) \in V_h \otimes \mathbb{R}^L_\diamond, \tag{5}$$

where the (discretized) conductivity σ_h lies in the discrete admissible set

$$\mathcal{A}_h = \{\sigma_h \in V_h : \lambda \leqslant \sigma_h \leqslant \lambda^{-1} \ \text{a.e. } \Omega\} = \mathcal{A} \cap V_h.$$

Then the discrete optimization problem reads

$$\min_{\sigma_h \in \mathcal{A}_h} \left\{ J_h(\sigma_h) = \tfrac{1}{2}\|U_h(\sigma_h) - U^\delta\|^2 + \alpha \Psi(\sigma_h) \right\}, \tag{6}$$

where the discrete penalty functional $\Psi(\sigma_h)$ is given by $\Psi(\sigma_h) = \frac{1}{2}\|\sigma_h\|^2_{H^1(\Omega)}$ and $\Psi(\sigma_h) = |\sigma_h|_{\mathrm{TV}(\Omega)}$ for the smoothness and total variation penalty, respectively.

Remark 3.1. In practice, even though the domain Ω is polyhedral, the electrode surfaces $\{e_l\}$ can still be curved, and this calls for the approximation of the surfaces $\{e_l\}$ by polyhedral surfaces in the discrete variational formulation. However, we defer relevant discussions to section 4.

We observe that, due to the use of linear finite elements, the box constraint on σ_h reduces to that on the nodal values, which greatly facilitates the solution of the resulting discrete optimization problem. Since the set $\mathcal{A}_h$ is finite dimensional and uniformly bounded, the compactness and the norm equivalence in finite-dimensional spaces immediately yields the

existence of a minimizer $\sigma_h^* \in \mathcal{A}_h$ to the discrete functional $J_h(\sigma_h)$ over the discrete admissible set $\mathcal{A}_h$ for any $h > 0$.

One basic question is whether the sequence $\{\sigma_h^*\}$ of discrete minimizers converges to a minimizer of the continuous functional $J(\sigma)$ as the mesh size h tends to zero. This issue is concerned with the validity of the approximation procedure, and hence it is of significant practical interest. To this end, we shall first establish a discrete analogue of lemma 2.2 on the approximation property of the discrete parameter-to-state map $\sigma_h \mapsto (u_h(\sigma_h), U_h(\sigma_h))$ to the continuous counterpart $\sigma \mapsto (u(\sigma), U(\sigma))$. The lemma will play a crucial role in establishing the desired convergence for polyhedral domains.

Lemma 3.1. *Let the sequence* $\{\sigma_h\}_{h>0} \subset \mathcal{A}_h \subset \mathcal{A}$ *converge in* $L^r(\Omega)$, $r \geqslant 1$, *to some* $\sigma \in \mathcal{A}$ *as h tends to zero. Then the sequence of finite element approximations* $\{(u_h(\sigma_h), U_h(\sigma_h))\}_{h>0}$ *converges to* $(u(\sigma), U(\sigma))$ *in* $\mathbb{H}$ *as h tends to zero.*

Proof. First recall the weak formulation of $(u, U) \equiv (u(\sigma), U(\sigma))$ and $(u_h, U_h) \equiv (u_h(\sigma_h), U_h(\sigma_h))$ in (2) and (5), respectively. It follows from Lax–Milgram theorem that both (u, U) and (u_h, U_h) are uniformly bounded in $\mathbb{H}$. By setting the test functions (v, V) and (v_h, V) in identities (2) and (5) to $(\mathcal{R}_h u - u_h, U - U_h) \in \mathbb{H}_h \subset \mathbb{H}$ and then subtracting them, we deduce

$$\begin{aligned}\int_\Omega \sigma_h |\nabla(u - u_h)|^2 \,\mathrm{d}x + \sum_{l=1}^{L} z_l^{-1} \int_{e_l} |u - u_h - U_l + U_{h,l}|^2 \,\mathrm{d}s \\ = -\int_\Omega (\sigma - \sigma_h)\nabla u \cdot \nabla(\mathcal{R}_h u - u_h)\,\mathrm{d}x + \int_\Omega \sigma_h \nabla(u - u_h)\cdot\nabla(u - \mathcal{R}_h u)\,\mathrm{d}x \\ + \sum_{l=1}^{L} z_l^{-1} \int_{e_l} (u - \mathcal{R}_h u)(u - u_h - U_l + U_{h,l})\,\mathrm{d}s := \mathrm{I} + \mathrm{II} + \mathrm{III}.\end{aligned}$$

It suffices to estimate the three terms (I, II and III) on the right-hand side. For the first term I, the generalized Hölder's inequality gives

$$|\mathrm{I}| \leqslant \|\sigma - \sigma_h\|_{L^p(\Omega)} \|\nabla u\|_{L^q(\Omega)} \|\nabla(\mathcal{R}_h u - u_h)\|_{L^2(\Omega)},$$

where the exponent $q > 2$ is from theorem 2.1, and the exponent p satisfies $p^{-1} + q^{-1} = 2^{-1}$. Further, we note that

$$\begin{aligned}\|\nabla(\mathcal{R}_h u - u_h)\|_{L^2(\Omega)} &\leqslant \|\nabla \mathcal{R}_h u\|_{L^2(\Omega)} + \|\nabla u_h\|_{L^2(\Omega)} \\ &\leqslant C(\|u\|_{H^1(\Omega)} + \|u_h\|_{H^1(\Omega)}) < C.\end{aligned}$$

By repeating the proof in lemma 2.2, we deduce that the first term $\mathrm{I} \to 0$ as h tends to zero. For the second term II, we deduce from the uniform bound of the discrete admissible set $\mathcal{A}_h$ that

$$\begin{aligned}\mathrm{II} &\leqslant \|\sigma_h\|_{L^\infty(\Omega)} \|\nabla(u - u_h)\|_{L^2(\Omega)} \|\nabla(u - \mathcal{R}_h u)\|_{L^2(\Omega)} \\ &\leqslant \lambda^{-1} \|\nabla(u - u_h)\|_{L^2(\Omega)} \|\nabla(u - \mathcal{R}_h u)\|_{L^2(\Omega)},\end{aligned}$$

which tends to zero in light of the approximation property of the operator $\mathcal{R}_h$ in (4) and uniform boundedness of $\|\nabla(u - u_h)\|_{L^2(\Omega)}$. The third term III follows analogously from the trace theorem [15]. These three estimates together with lemma 2.1 yield the desired assertion. □

Now we can state the first main result, i.e., the convergence of finite element approximations $\{\sigma_h^*\}$ on polyhedral domains.

Theorem 3.1. *Let $\{\sigma_h^* \in \mathcal{A}_h\}_{h>0}$ be a sequence of minimizers to the discrete optimization problem (6). Then it contains a subsequence convergent to a minimizer of problem (3) as h tends to zero.*

(a) The convergence is weakly in $H^1(\Omega)$, if $\Psi(\sigma_h) = \frac{1}{2}\|\sigma_h\|^2_{H^1(\Omega)}$.
(b) The convergence is in $L^1(\Omega)$, if $\Psi(\sigma_h) = |\sigma_h|_{\mathrm{TV}(\Omega)}$.

Proof. First we note that the constant function $\sigma_h \equiv 1$ belongs to the discrete admissible set $\mathcal{A}_h$ for all h. The minimizing property of σ_h^* indicates that the sequence of functional values $\{J_h(\sigma_h^*)\}$ is uniformly bounded. Thus the sequence $\{\Psi(\sigma_h^*)\}$ is uniformly bounded, and there exists a subsequence, again denoted by $\{\sigma_h^*\}$, and some $\sigma^* \in \mathcal{A}$, such that $\sigma_h^* \to \sigma^*$ weakly either in $H^1(\Omega)$ or $\mathrm{BV}(\Omega)$. By lemma 2.3, we have $\sigma_h^* \to \sigma^*$ in $L^1(\Omega)$, which together with lemma 3.1 implies

$$(u_h(\sigma_h^*), U(\sigma_h^*)) \to (u(\sigma^*), U(\sigma^*)) \quad \text{in } \mathbb{H} \text{ as } h \to 0.$$

Meanwhile, the weak lower semicontinuity of norms implies $\Psi(\sigma^*) \leqslant \liminf_{h\to 0} \Psi(\sigma_h^*)$. Altogether, we derive

$$\begin{aligned} J(\sigma^*) &= \tfrac{1}{2}\|U(\sigma^*) - U^\delta\|^2 + \alpha\Psi(\sigma^*) \\ &\leqslant \lim_{h\to 0} \tfrac{1}{2}\|U_h(\sigma_h^*) - U^\delta\|^2 + \liminf_{h\to 0} \alpha\Psi(\sigma_h^*) \\ &\leqslant \liminf_{h\to 0} \left(\tfrac{1}{2}\|U_h(\sigma_h^*) - U^\delta\|^2 + \alpha\Psi(\sigma_h^*)\right) = \liminf_{h\to 0} J_h(\sigma_h^*). \end{aligned} \tag{7}$$

Now we discuss the two penalties separately. First we consider the case $\Psi(\sigma) = \frac{1}{2}\|\sigma\|^2_{H^1(\Omega)}$. For any $\sigma \in \mathcal{A}$, the density of the space $C^\infty(\overline{\Omega})$ in the space $H^1(\Omega)$ [15] implies the existence of a sequence $\{\sigma^\epsilon\} \subset C^\infty(\overline{\Omega}) \cap \mathcal{A}$ such that

$$\lim_{\epsilon\to 0^+} \|\sigma^\epsilon - \sigma\|_{H^1(\Omega)} = 0. \tag{8}$$

The minimizing property of σ_h^* gives $J_h(\sigma_h^*) \leqslant J_h(\mathcal{I}_h\sigma^\epsilon)$ for any $\epsilon > 0$. Letting h to zero, and appealing to the property of interpolation operator $\mathcal{I}_h$, lemma 3.1 and (7) yield $J(\sigma^*) \leqslant J(\sigma^\epsilon)$. Since ϵ is arbitrary, by letting ϵ to zero, noting the approximation property of the sequence σ^ϵ in (8), and the continuity result in lemma 2.2, we deduce that $J(\sigma^*) \leqslant J(\sigma)$ for any $\sigma \in \mathcal{A}$. This shows the desired assertion for $\Psi(\sigma) = \frac{1}{2}\|\sigma\|^2_{H^1(\Omega)}$.

Next we consider the case $\Psi(\sigma) = |\sigma|_{\mathrm{TV}(\Omega)}$. For any $\sigma \in \mathcal{A}$, lemma 2.4 implies the existence of a sequence $\{\sigma^\epsilon\} \subset C^\infty(\overline{\Omega})$ such that $\int_\Omega |\sigma^\epsilon - \sigma|\,\mathrm{d}x < \epsilon$ and $|\int_\Omega |\nabla\sigma^\epsilon|\,\mathrm{d}x - \int_\Omega |D\sigma|| < \epsilon$. Next we define $\tilde{\sigma}_\epsilon = P_{[\lambda,\lambda^{-1}]}\sigma^\epsilon$, where the operator $P_{[\lambda,\lambda^{-1}]}$ denotes pointwise projection. Since $\nabla\tilde{\sigma}^\epsilon = \nabla\sigma^\epsilon\chi_{\Omega_\epsilon}$ (with the set $\Omega_\epsilon = \{x \in \Omega : \lambda \leqslant \sigma^\epsilon \leqslant \lambda^{-1}\}$), which is uniformly bounded, and thus $\tilde{\sigma}^\epsilon \in \mathcal{A} \cap W^{1,\infty}(\Omega)$. With the choice $\sigma_h = \mathcal{I}_h\tilde{\sigma}^\epsilon \in V_h$, the minimizing property of $\sigma_h^* \in \mathcal{A}_h$ gives $J_h(\sigma_h^*) \leqslant J_h(\mathcal{I}_h\tilde{\sigma}^\epsilon)$ for any $\epsilon > 0$. By the approximation property of the operator $\mathcal{I}_h$ in (4) and the fact that $\tilde{\sigma}^\epsilon \in W^{1,\infty}(\Omega)$, we deduce

$$\lim_{h\to 0} \mathcal{I}_h\tilde{\sigma}^\epsilon = \tilde{\sigma}^\epsilon \quad \text{in } W^{1,1}(\Omega).$$

Letting h to zero, and appealing to lemma 3.1 and (7) yield $J(\sigma^*) \leqslant J(\tilde{\sigma}^\epsilon)$. We observe the following approximation properties of the sequence $\tilde{\sigma}^\epsilon$,

$$\int_\Omega |\nabla \tilde{\sigma}^\epsilon| \, \mathrm{d}x = \int_{\Omega_\epsilon} |\nabla \sigma^\epsilon| \, \mathrm{d}x \leqslant \int_\Omega |\nabla \sigma^\epsilon| \, \mathrm{d}x \leqslant \int_\Omega |D\sigma| + \epsilon,$$
$$\int_\Omega |\tilde{\sigma}^\epsilon - \sigma| \, \mathrm{d}x \leqslant \int_\Omega |\sigma^\epsilon - \sigma| \, \mathrm{d}x < \epsilon,$$

where the last line follows from the contraction property of the operator $P_{[c_0,c_1]}$. By letting ϵ to zero and the continuity result in lemma 2.2, we deduce $J(\sigma^*) \leqslant J(\sigma)$ for any $\sigma \in \mathcal{A}$, i.e., σ^* is indeed a minimizer to the functional $J(\sigma)$. This concludes the proof of the theorem. □

Remark 3.2. A close inspection of the proof of theorem 3.1 indicates that with minor modifications the result holds also for the continuum model, provided that the input current j satisfies a certain regularity condition so that an analogue of theorem 2.1 is valid, cf [21, appendix A]. Further, the analysis can be easily adapted to multi-parameter models, e.g., $\Psi(\sigma) = \frac{1}{2}\|\sigma\|^2_{H^1(\Omega)} + \gamma\|\sigma\|_{L^1(\Omega)}$.

4. Convergence for smooth curved domains

Now we turn to the convergence analysis of finite element approximations on convex smooth curved domains. In the finite element literature, there are several different ways to treat curved domains, e.g., isoparametric elements [10] and curved elements [3]. In EIT imaging algorithms, we usually approximate the domain Ω with a polyhedral domain Ω_h (with its boundary denoted by Γ_h), and solve the forward problem (1) directly on the polyhedral domain Ω_h, with the resulting solution taken as the desired approximation. That is, all computations are performed on a polyhedral domain Ω_h. Such a discretization strategy has been routinely employed in the implementation of EIT imaging techniques, but to the best of our knowledge, it has not been rigorously justified.

Throughout, the triangulation $\mathcal{T}_h$ is shape regular and quasi-uniform and it consists of simplicial elements, and the finite element space V_h is the canonical piecewise linear finite element space defined on $\mathcal{T}_h$. Further, we make the following assumption on the domain Ω and the polyhedral approximation Ω_h (with their boundaries being Γ and Γ_h, respectively). The finite element space V_h will be used to discretize both the forward model and the conductivity distribution.

Assumption 4.1. *The domain Ω is convex with a C^2 boundary Γ. The approximating polyhedral domain Ω_h is also convex, and the vertices of Γ_h are on the boundary Γ.*

Remark 4.1. The convexity and smoothness in assumption 4.1 are mainly for three-dimensional (3D) domains. In the two-dimensional (2D) case, the discussions below work for domains with a piecewise smooth boundary; see e.g. [6]. That is, the convexity of the domain is not required then.

To ease the exposition, we introduce some further notation. By assumption 4.1, clearly there holds the relation $\Omega_h \subset \Omega$. Due to the convexity of the domain Ω_h, we can define a projection operator ϕ_h by

$$\phi_h : \ \overline{\Omega}\backslash\Omega_h \mapsto \Gamma_h,$$
$$\phi_h(x) = \operatorname{argmin}_{z\in\Gamma_h}|x - z|.$$

We denote by ϕ_h^1 and ϕ_h^2 the map ϕ_h restricted to the interior domain $\Omega\backslash\overline{\Omega}_h$ and the boundary Γ, respectively, i.e., $\phi_h^1 = \phi_h|_{\Omega\backslash\overline{\Omega}_h}$ and $\phi_h^2 = \phi_h|_\Gamma$. Next let S_h be any finite element surface

(of the triangulation $\mathcal{T}_h$) of the polyhedral domain Ω_h lying on Γ_h, and T_h be the finite element to which S_h belongs. We denote the pair by (S_h, T_h), and by $(\phi_h^1)^{-1}(S_h)$ the preimage of S_h under ϕ_h^1. Then there holds $\Omega\backslash\overline{\Omega}_h \subset \cup_{S_h}(\phi_h^1)^{-1}(S_h)$. Further for any interior point x_h to the surface S_h (understood elementwise), we can define a unit outward normal vector n_{x_h} through x_h, which is perpendicular to S_h. Due to the convexity of the domain Ω, the outward normal vector n_{x_h} intersects the boundary Γ uniquely at a point x. This defines a map

$$\begin{aligned}\psi_h : \quad & \cup_{S_h} \operatorname{int} S_h \mapsto \Gamma,\\ & \psi_h(x_h) = x.\end{aligned}$$

Furthermore, by the convexity of the domain Ω_h, Ω_h lies on only one side of any plane that contains S_h, and therefore, $\phi_h^2(\psi_h(x_h)) = x_h$, $x_h \in \operatorname{int} S_h$. For any surface patch $e \subset \Gamma$, there holds

$$\phi_h^2(e) = \cup S_{e,h}, \tag{9}$$

where $S_{e,h} = S_h \cap \phi_h^2(e)$. We denote the subset $\cup_{x\in\operatorname{int} S_{e,h}}\psi_h(x) \subset e$ by $\varrho_h(e)$, which will be taken as an approximation to the surface electrode e in the convergence analysis.

The following lemma provides some estimates on the domain approximation under assumption 4.1. These estimates are crucial to subsequent convergence analysis.

Lemma 4.1. *Let assumption 4.1 be fulfilled. Then for any small h, the following statements hold.*

(i) The distance $d(\Gamma, \Gamma_h) := \sup_{x\in\Gamma}\inf_{x_h\in\Gamma_h}|x - x_h|$ *between the boundaries* Γ *and* Γ_h *converges to zero at* $d(\Gamma, \Gamma_h) \leqslant Ch^2$.

(ii) The unit outward normal vector $n(\phi_h^2(x))$ *for* $\phi_h^2(x)$ *to* Γ_h *converges to that at x to the boundary* Γ *at* $|n(x) - n(\phi_h^2(x))| \leqslant Ch$.

(iii) The measure $|\Gamma_h|$ *converges to* $|\Gamma|$, *i.e.,* $||\Gamma| - |\Gamma_h|| \leqslant Ch$.

Proof. We discuss only the 3D case, since the treatment of the 2D case is straightforward (cf [6]). By the C^2 regularity of the boundary Γ from assumption 4.1, the unit outward normal vector $n : \Gamma \mapsto \mathbb{S}^2$ is Lipschitz continuous with a Lipschitz constant L, i.e., $|n(x) - n(y)| \leqslant L|x - y|$.

Now for any fixed $x \in \Gamma$, $d(x, \Gamma_h)$ in assertions (i) and (ii) does not depend on the choice of the coordinate system, and hence we may assume $n(x) = (0, 0, 1)^{\mathrm{t}}$. The implicit function theorem ensures the existence of a neighborhood $\mathcal{N}_x \subset \Gamma$ of x such that $x_3 = f(x_1, x_2)$ in $\mathcal{N}_x$ for some $f \in C^2$. In particular, we many choose the set $\mathcal{N}_x = \{z \in \Gamma : |z - x| < L^{-1}\}$. To see this, it suffices to show that any line parallel to the normal vector $n(x) = (0, 0, 1)^{\mathrm{t}}$ intersects $\mathcal{N}_x$ at most once, which we prove by contradiction. Suppose that the boundary Γ is defined by $F(x) = 0$. The definition of $\mathcal{N}_x$ implies that for any $z \in \mathcal{N}_x$, $|n(z) - n(x)| \leqslant 1$, i.e., $n(z) \cdot n(x) \geqslant \frac{1}{2}$ and hence $\frac{\partial F}{\partial x_3}|_z > 0$. Now assume the contrary, i.e., there are two points $(x_1, x_2, \tilde{x}_3)$ and $(x_1, x_2, \hat{x}_3)$ in $\mathcal{N}_x$ with $\tilde{x}_3 < \hat{x}_3$. The tangent plane at point $\tilde{x} := (x_1, x_2, \tilde{x}_3)$ is given by

$$\{z = (z_1, z_2, z_3) : (z - \tilde{x}) \cdot \nabla F(\tilde{x}) = 0\}.$$

By the choice of the outward normal $n(\tilde{x})$ and the convexity of the domain Ω, the surface Γ lies below the tangent plane, i.e., $(z - \tilde{x}) \cdot \nabla F(\tilde{x}) \leqslant 0$ for all $z \in \Gamma$, which contradicts the strictly reverse inequality for the point $(x_1, x_2, \hat{x}_3)$. This shows the desired assertion on the choice of the neighborhood $\mathcal{N}_x$.

Note that for any $z \in \mathcal{N}_x$, we have $n(z) \cdot n(x) > \frac{1}{2}$ and hence $f_1^2(z) + f_2^2(z) < 1$, where $f_i = \frac{\partial f}{\partial x_i}$, $i = 1, 2$. Hence there holds $|x - z|^2 = |x_1 - z_1|^2 + |x_2 - z_2|^2 + |f(x_1, x_2) -$

$f(z_1, z_2)|^2$ and by the mean value theorem, $f(x_1, x_2) - f(z_1, z_2) = (x_1 - z_1)f_1(\xi_1) + (x_2 - z_2)f_2(\xi_2)$, where the point (ξ_1, ξ_2) lies on the line segment from (x_1, x_2) to (z_1, z_2). Consequently, $|f(x_1, x_2) - f(z_1, z_2)|^2 \leqslant 2(|x_1 - z_1|^2 + |x_2 - z_2|^2)$. Moreover $|x - z|^2 \leqslant 3(|x_1-z_1|^2+|x_2-z_2|^2)$, and we can conclude that the set $\{(y_1, y_2) : |x_1-y_1|^2+|x_2-y_2|^2 \leqslant \frac{1}{3L^2}\}$ is a subset of the projection of the set $\mathcal{N}_x$ to the x_1–x_2 plane.

Now suppose that h is sufficiently small. Consider the projection of x onto the x_1–x_2 plane, which intersects some triangle $\triangle ABC$, with $A, B, C \in \mathcal{N}_x$ being vertices on the polyhedral boundary Γ_h. Therefore, there is a surface patch $\widehat{\mathcal{N}}_x \subset \mathcal{N}_x$ (with $x \in \widehat{\mathcal{N}}_x$) and $\triangle ABC$ can be respectively represented by $(x_1, x_2, f(x_1, x_2))$ and $(x_1, x_2, f_h(x_1, x_2))$ with f and f_h being C^2 continuous and affine, respectively. We note that by the construction in the preceding paragraph, such a representation also exists for the neighboring elements. Let $n(A)$ be the unit outward normal vector at the vertex $A \in \widehat{\mathcal{N}}_x$ to the surface Γ, and n_{ABC} be that of the triangle $\triangle ABC$. Then there holds

$$n(A) = \left(f_1^2 + f_2^2 + 1\right)^{-\frac{1}{2}}(-f_1, -f_2, 1)|_A,$$
$$n_{ABC} = \left(f_{1,h}^2 + f_{2,h}^2 + 1\right)^{-\frac{1}{2}}(-f_{1,h}, -f_{2,h}, 1)|_{ABC},$$

where $f_{i,h} = \frac{\partial f_h}{\partial x_i}|_{ABC}$, $i = 1, 2$. Now the C^2 regularity of f yields

$$\begin{aligned} x_{3,B} - x_{3,A} &= f(x_{1,B}, x_{2,B}) - f(x_{1,A}, x_{2,A}) \\ &= f_1|_A(x_{1,B} - x_{1,A}) + f_2|_A(x_{2,B} - x_{2,A}) + O(h^2). \end{aligned}$$

Consequently, the inner product $|n(A) \cdot \overrightarrow{BA}|$ can be bounded by

$$|n(A) \cdot \overrightarrow{BA}| = \left|\left(f_1^2 + f_2^2 + 1\right)^{-\frac{1}{2}}(-f_1, -f_2, 1)\big|_A \cdot [x_{1,B}-x_{1,A} \;\; x_{2,B}-x_{2,A} \;\; x_{3,B}-x_{3,A}]\right| \leqslant Ch^2.$$

Similarly, one can deduce $|n(A) \cdot \overrightarrow{CA}| \leqslant Ch^2$. By the quasi-uniformity of the triangulation $\mathcal{T}_h$, the angle $\angle BAC$ is strictly bounded from below by zero, $|AB| \approx h$ and $|AC| \approx h$, and hence the inner product between $n(A)$ and any unit vector in the plane ABC is of the order $O(h)$. The normal vector $n(A)$ can be expressed as $n(A) = \alpha n_{ABC} + n_{ABC}^{\perp}$ with $n_{ABC}^{\perp} \perp n_{ABC}$ and $\alpha \in (0, 1)$ (due to the choice of orientation). Taking inner products both sides with $n_{ABC}^{\perp}$ yields

$$n(A) \cdot n_{ABC}^{\perp} = |n_{ABC}^{\perp}|^2$$

i.e., $|n_{ABC}^{\perp}| = O(h)$ and $\alpha = 1 - O(h)$. Hence, $|n(A) - n_{ABC}|^2 = (1-\alpha)^2 + |n_{ABC}|^2 = O(h^2)$, i.e., $|n(A) - n_{ABC}| \leqslant Ch$. It follows immediately from this estimate that

$$|f_1(A) - f_{1,h}| \leqslant Ch \quad \text{and} \quad |f_2(A) - f_{2,h}| \leqslant Ch.$$

With these preliminaries, now we can prove the assertions.

Proof of assertion (i). For any point $\bar{x} = (x_1, x_2, f(x_1, x_2)) \in \triangle ABC$, there holds $|x_1 - x_{1,A}| + |x_2 - x_{2,A}| \leqslant Ch$, and further

$$\begin{aligned} f(x_1, x_2) &= f(x_{1,A}, x_{2,A}) + (x_1 - x_{1,A})f_1(A) + (x_2 - x_{2,A})f_2(A) + O(h^2), \\ f_h(x_1, x_2) &= f_h(x_{1,A}, x_{2,A}) + (x_1 - x_{1,A})f_{1,h} + (x_2 - x_{2,A})f_{2,h}. \end{aligned}$$

Upon noting the identity $f(x_{1,A}, x_{2,A}) = f_h(x_{1,A}, x_{2,A})$, we deduce

$$|f(x_1, x_2) - f_h(x_1, x_2)| \leqslant |x_1 - x_{1,A}||f_1(A) - f_{1,h}| + |x_2 - x_{2,A}||f_2(A) - f_{2,h}| + Ch^2 \leqslant Ch^2.$$

Therefore $d(\bar{x}, \Gamma_h) \leqslant |f(x_1, x_2) - f_h(x_1, x_2)| \leqslant Ch^2$ and assertion (i) follows.

Proof of assertion (ii). It follows from the Lipschitz continuity of the unit normal vector $n(x)$ that

$$|n(x) - n_{ABC}| \leqslant |n(x) - n(A)| + |n(A) - n_{ABC}| \leqslant L|x - x_A| + Ch \leqslant Ch. \tag{10}$$

Now we distinguish the following cases. Case (a): $\phi_h^2(x) \in \triangle ABC$, then the assertion follows directly from (10) and the fact that $n(\phi_h^2(x)) = n_{ABC}$. Case (b): $\phi_h^2(x) \notin \triangle ABC$. By part (i), $|x - \phi_h^2(x)| = d(x, \Gamma_h) \leqslant Ch^2$, i.e., $\phi_h^2(x)$ lies within an $O(h^2)$ neighborhood of the point x. Let $\bar{x} \in \triangle ABC$ be the intersection point defined by the projection through the point $x \in \Gamma$ onto the x_1–x_2 plane. Then by the triangle inequality, $|\bar{x} - \phi_h^2(x)| \leqslant Ch^2$. Then the C^2 regularity of f yields $|x - \check{\phi}_h^2(x)| \leqslant Ch^2$, where $\check{\phi}_h^2(x)$ denotes the pull-back of the orthogonal projection of $\phi_h^2(x)$ (onto the x_1–x_2 plane) to the boundary Γ. The Lipschitz continuity of the normal vector, (10) and the triangle inequality yield

$$\left|n(x) - n\big(\phi_h^2(x)\big)\right| \leqslant \left|n(x) - n\big(\check{\phi}_h^2(x)\big)\right| + \left|n\big(\check{\phi}_h^2(x)\big) - n\big(\phi_h^2(x)\big)\right| \leqslant Ch.$$

This completes the proof of assertion (ii).

Proof of assertion (iii). Here we first consider a local patch. For any subset $\mathcal{N} \subset \mathcal{N}_x$ (with the choice $n(x) = (0, 0, 1)^{\mathrm{t}}$) with a boundary $\partial\mathcal{N}$ of finite perimeter, let $\mathcal{N}_h \subset \Gamma_h$ be the approximation of $\mathcal{N}$ which consists of triangles with all vertices lying on $\mathcal{N}$, and $\mathcal{N}_{x_1,x_2} \subset \mathbb{R}^2$ be the orthogonal projection of $\mathcal{N}_h$ onto the x_1–x_2 plane. According to the preceding construction, the projection is well defined. Then for any $(x_1, x_2) \in \mathcal{N}_{x_1,x_2}$, $(x_1, x_2, f_h(x_1, x_2)) \in \mathcal{N}_h$ and $(x_1, x_2, f(x_1, x_2)) \in \mathcal{N}$. Now for any triangle $\triangle ABC \subset \mathcal{N}_h$, $f_{i,h}|_{\triangle ABC}$ is constant, and consequently

$$|f_i|_{(x_1,x_2)} - f_{i,h}|_{(x_1,x_2)}| \leqslant |f_i|_{(x_1,x_2)} - f_i|_A| + |f_i|_A - f_{i,h}|_A| \leqslant Ch.$$

Let $\widetilde{\mathcal{N}} = \{(x_1, x_2, f(x_1, x_2)) : (x_1, x_2) \in \mathcal{N}_{x_1,x_2}\} \subset \mathcal{N}$. Then

$$|\widetilde{\mathcal{N}}| = \int_{\mathcal{N}_{x_1,x_2}} \sqrt{f_1^2 + f_2^2 + 1}\, \mathrm{d}x_1\, \mathrm{d}x_2 \quad \text{and} \quad |\mathcal{N}_h| = \int_{\mathcal{N}_{x_1,x_2}} \sqrt{f_{1,h}^2 + f_{2,h}^2 + 1}\, \mathrm{d}x_1\, \mathrm{d}x_2,$$

where the derivatives $f_{i,h}$ should be understood elementwise. Therefore,

$$||\widetilde{\mathcal{N}}| - |\mathcal{N}_h|| \leqslant \int_{\mathcal{N}_{x_1,x_2}} |f_1 - f_{1,h}| + |f_2 - f_{2,h}| \leqslant Ch.$$

Moreover, since the mesh size is h, and the surface Γ is C^2, the set $\mathcal{N}\backslash\widetilde{\mathcal{N}}$ is contained in the set $\{x : d(x, \partial\mathcal{N}) \leqslant Ch\}$. Consequently, we have

$$||\mathcal{N}| - |\mathcal{N}_h|| \leqslant ||\widetilde{\mathcal{N}}| - |\mathcal{N}_h|| + |\mathcal{N}\backslash\widetilde{\mathcal{N}}| \leqslant Ch.$$

Now we estimate the approximation of the whole boundary. Since the boundary Γ is compact and $\Gamma \subset \cup_{x\in\Gamma}\mathcal{N}_x$, by the Heine–Borel theorem, there exists a finite number of points $\{x^i\}_{i=1}^n$ such that $\Gamma \subset \cup_{x^i}\mathcal{N}_{x^i}$. Let $\mathcal{N}^1 = \mathcal{N}_{x^1}$, $\mathcal{N}^2 = \mathcal{N}_{x^2}\backslash\mathcal{N}^1$, $\mathcal{N}^i = \mathcal{N}_{x^i}\backslash \cup_{j=1}^{i-1} \mathcal{N}^j$, $i = 3, \ldots, n$. Then each set $\mathcal{N}_{x^i}$ has a boundary of finite measure. Clearly there holds $|\Gamma| = \sum_i |\mathcal{N}^i|$ and $|\Gamma_h| \geqslant \sum_i |\mathcal{N}_h^i|$. Now by the nonexpansiveness of the map ϕ_h^2, there holds $|\Gamma_h| \leqslant |\Gamma|$. Now assertion (iii) follows from

$$|\Gamma| - |\Gamma_h| \leqslant \sum_i \left||\mathcal{N}^i| - \left|\mathcal{N}_h^i\right|\right| \leqslant Ch.$$

This completes the proof of the lemma. □

Remark 4.2. The quasi-uniformity of the mesh is essential for lemma 4.1. One can find a counterexample on the approximation of surface area in [16, section 623] in the absence of the quasi-uniformity condition; see also [16, sections 624 and 627] for related discussions. Further, the constant C in lemma 4.1 depends on the curvature of the boundary.

With the help of lemma 4.1, we can show the following properties of the maps ϕ_h^1, ϕ_h^2 and ϱ_h defined at the beginning of this section, which are crucial for the convergent analysis below.

Lemma 4.2. *Let assumption 4.1 be fulfilled. Then there exists a function* $\epsilon_h \to 0$ *as* $h \to 0$ *such that the maps* ϕ_h^1, ϕ_h^2 *and* ϱ_h *satisfy:*

(i) For any element S_h, *there holds* $\frac{|(\phi_h^1)^{-1}(S_h)|}{|T_h|} \leqslant \epsilon_h$.

(ii) For any subset $e \subset \Gamma$, *there holds* $|\phi_h^2(e)| \leqslant |e|$, $|\phi_h^2(e)| \to |e|$ *and* $|\phi_h^2(e)| \leqslant |\varrho_h(e)| \leqslant (1+\epsilon_h)|\phi_h^2(e)|$.

Proof. By definition, there holds $|\phi_h^1(x) - x| \leqslant d(\Gamma, \Gamma_h)$, and $(\phi_h^1)^{-1}(S_h) \subset \{x \in \Omega \setminus \Omega_h : d(x, S_h) \leqslant d(\Gamma, \Gamma_h)\}$. Hence, for any S_h, the measure of the set $\{x \in \Omega \setminus \Omega_h : d(x, S_h) \leqslant d(\Gamma, \Gamma_h)\}$ satisfies $|\{x \in \Omega \setminus \Omega_h : d(x, S_h) \leqslant d(\Gamma, \Gamma_h)\}| \leqslant Ch^{d+1}$, in view of lemma 4.1 (i) and the fact $|S_h| \approx h^{d-1}$, and the quasi-uniformity of $\mathcal{T}_h$ implies $|T_h| \approx h^d$, from which assertion (i) follows directly.

Since the map ϕ_h^2 is nonexpansive, $|\phi_h^2(e)| \leqslant |e|$ and $|\phi_h^2(e)| = |\phi_h^2(\varrho_h(e))| \leqslant |\varrho_h(e)|$. Meanwhile, clearly there holds $|e| - |\phi_h^2(e)| \leqslant |\Gamma| - |\Gamma_h|$, and consequently $|\phi_h^2(e)| \to |e|$ by lemma 4.1 (iii). Now by lemma 4.1 (ii) we have $\delta_h = \sup_x |n_x - n_{\phi_h^2(x)}| \leqslant Ch$. Without loss of generality, we can assume that $\phi_h^2(e) \subset \operatorname{int} S_h$. By using a local coordinate system, let S_h be in the x_1–x_2 plane (x_1 axis in the 2D case). Then the set $\varrho_h(e) \subset \psi_h(\operatorname{int} S_h)$ can be represented by a nonnegative function $f(x_1, x_2)$ for $(x_1, x_2) \in \operatorname{int} S_h$. It follows from the definition of δ_h that

$$\left| \frac{(f_1, f_2, 1)}{\sqrt{1 + f_1^2 + f_2^2}} - (0, 0, 1) \right| \leqslant \delta_h,$$

from which it follows that $f_1^2 + f_2^2 \leqslant \frac{\delta_h^2}{1-\delta_h^2}$. However, the area for the patch $\varrho_h(e)$ is given by

$$|\varrho_h(e)| = \int_{\phi_h^2(e)} \sqrt{1 + f_1^2 + f_2^2}\, \mathrm{d}x\, \mathrm{d}y \leqslant \left(1 + \frac{\delta_h}{\sqrt{1-\delta_h^2}}\right) |\phi_h^2(e)|.$$

This shows the second assertion. Then ϵ_h can be properly chosen to satisfy both (i) and (ii). □

We shall also need the following lemma.

Lemma 4.3. *Let* $p \geqslant 1$ *and the domain* Ω *divide into* n *disjoint open subdomains* $\{\Omega_i\}$, *with a Lipschitz interface between every neighboring subdomains. Then* $u|_{\Omega_i} \in W^{1,p}(\Omega_i)$ *and* $u \in C(\overline{\Omega})$ *imply* $u \in W^{1,p}(\Omega)$.

Proof. It suffices to consider the case $n = 2$, i.e., two domains Ω_1 and Ω_2 with the interface being $\Gamma_{1,2}$. We define functions v_j, $j = 1, \ldots, d$, by $v_j(x) = \frac{\partial u}{\partial x_j} \chi_{\Omega_1 \cup \Omega_2}$. Then for any $\phi \in C_0^\infty(\Omega)$, we have

$$\int_\Omega v_j \phi \, \mathrm{d}x = \int_{\Omega_1} v_j \phi \, \mathrm{d}x + \int_{\Omega_2} v_j \phi \, \mathrm{d}x = -\int_{\Omega_1} u \phi_{x_j} \, \mathrm{d}x - \int_{\Omega_2} u \phi_{x_j} \, \mathrm{d}x + \int_{\Gamma_{1,2}} [u\phi] n_{x_j} \, \mathrm{d}s,$$

where $[\cdot]$ denotes the jump across the interface $\Gamma_{1,2}$ and n_{x_j} is the jth component of the unit outward normal vector to the boundary $\partial\Omega_1$. By the continuity of u, the jump term on the interface $\Gamma_{1,2}$ vanishes identically, and thus $\int_\Omega v_j \phi \, \mathrm{d}x = -\int_\Omega u \phi_{x_j} \, \mathrm{d}x$, i.e., v_j is the weak derivative of u. Clearly, the function v_j belongs to the space $L^p(\Omega)$. This concludes the proof of the lemma. □

The finite element solution is only defined on the domain Ω_h, whereas the true solution is defined on the domain Ω. In order to compare them, we introduce an extension operator $\jmath : \Omega_h \mapsto \Omega$ as follows:

$$\jmath v_h(x) = \begin{cases} v_h(x), & x \in \overline{\Omega}_h, \\ v_h(\phi_h(x)), & x \in \overline{\Omega}\backslash\overline{\Omega}_h, \end{cases} \quad \forall v_h \in V_h. \tag{11}$$

The extension operator $\jmath$ satisfies the following estimate.

Lemma 4.4. *Let $p \geqslant 1$ and assumption 4.1 be fulfilled. Then there holds*

$$\|\jmath v_h\|_{W^{1,p}(\Omega\backslash\Omega_h)} \leqslant C\epsilon_h^{\frac{1}{p}} \|v_h\|_{W^{1,p}(\Omega_h)} \quad \forall v_h \in V_h.$$

Proof. Clearly, $\jmath v_h \in C(\overline{\Omega})$ and the projection operator ϕ_h is nonexpansive, i.e., $|\phi_h(x) - \phi_h(y)| \leqslant |x - y|$. Thus for any $x \in \Omega\backslash\overline{\Omega}_h$ with $\phi_h(x) \in S_h \subset T_h$, $T_h \in \mathcal{T}_h$, there holds

$$\begin{aligned} |\nabla \jmath v_h(x)| &= \limsup_{y\to x} \frac{|\jmath v_h(x) - \jmath v_h(y)|}{|x-y|} \\ &\leqslant \limsup_{\substack{y\to x \\ \phi_h(y)\neq\phi_h(x)}} \frac{|v_h(\phi_h(x)) - v_h(\phi_h(y))|}{|\phi_h(x) - \phi_h(y)|} \leqslant \|\nabla v_h\|_{L^\infty(S_h)}, \end{aligned}$$

and

$$|\jmath v_h(x)| = |v_h(\phi_h(x))| \leqslant \|v_h\|_{L^\infty(S_h)}.$$

Further, $\|\nabla v_h\|_{L^\infty(S_h)} \leqslant \|\nabla v_h\|_{L^\infty(T_h)}$ and $\|v_h\|_{L^\infty(S_h)} \leqslant \|v_h\|_{L^\infty(T_h)}$, and thus,

$$\begin{aligned} \|\nabla \jmath v_h\|^p_{L^p((\phi_h^1)^{-1}(S_h))} &\leqslant |(\phi_h^1)^{-1}(S_h)| \|\nabla v_h\|^p_{L^\infty(T_h)}, \\ \|\jmath v_h\|^p_{L^p((\phi_h^1)^{-1}(S_h))} &\leqslant |(\phi_h^1)^{-1}(S_h)| \|v_h\|^p_{L^\infty(T_h)}. \end{aligned} \tag{12}$$

Now for the element $T_h \in \mathcal{T}_h$, we consider an affine transformation $\mathcal{F} : \widehat{T} \mapsto T_h$, $\mathcal{F}(\hat{x}) = J\hat{x}+b$, where $\widehat{T}$ is the reference element. The quasi-uniformity of the triangulation $\mathcal{T}_h$ implies [10]

$$|\det(J)| = |T_h|/|\widehat{T}| \approx h^d, \quad \|J\| \approx h, \quad \|J^{-1}\| \approx h^{-1}. \tag{13}$$

where $\approx$ means being of the same order, and $\|\cdot\|$ is the matrix spectral norm. Then by a change of variable, chain rule and (13), we deduce that for any $s \geqslant 0$

$$|\widehat{v}|_{W^{s,p}(\widehat{T})} \approx \begin{cases} h^{s-\frac{d}{p}} |v|_{W^{s,p}(T_h)}, & 1 \leqslant p < \infty, \\ h^s |v|_{W^{s,p}(T_h)}, & p = \infty. \end{cases}$$

Consequently, we have

$$\begin{aligned} |v_h|^p_{W^{1,\infty}(T_h)} &\approx h^{-p} |\widehat{v}_h|^p_{W^{1,\infty}(\widehat{T})} \approx h^{-p} |\widehat{v}_h|^p_{W^{1,p}(\widehat{T})} \\ &\approx h^{-d} |v_h|^p_{W^{1,p}(T_h)} \approx \frac{1}{|T_h|} |v_h|^p_{W^{1,p}(T_h)}, \\ |v_h|^p_{L^\infty(T_h)} &\approx |\widehat{v}_h|^p_{L^\infty(\widehat{T})} \approx |\widehat{v}_h|^p_{L^p(\widehat{T})} \\ &\approx h^{-d} |v_h|^p_{L^p(T_h)} \approx \frac{1}{|T_h|} |v_h|^p_{L^p(T_h)}. \end{aligned}$$

This together with (12) yields

$$\begin{aligned} \|\nabla \jmath v_h\|^p_{L^p((\phi_h^1)^{-1}(S_h))} &\leqslant C \frac{\left|\left(\phi_h^1\right)^{-1}(S_h)\right|}{|T_h|} \|\nabla v_h\|^p_{L^p(T_h)}, \\ \|\jmath v_h\|^p_{L^p((\phi_h^1)^{-1}(S_h))} &\leqslant C \frac{\left|\left(\phi_h^1\right)^{-1}(S_h)\right|}{|T_h|} \|v_h\|^p_{L^p(T_h)}. \end{aligned}$$

Now summing overall S_h and part (i) of lemma 4.2 yield the desired assertion. □

The next result estimates the error of the boundary term.

Lemma 4.5. *Let assumption 4.1 be fulfilled. Then for any $v_h \in V_h$, a subset $e_h \subset \operatorname{int} S_h$, and $\tilde{e}_h = \psi_h(e_h)$, there holds*

$$\left| \int_{e_h} v_h \,\mathrm{d}s - \int_{\tilde{e}_h} \jmath v_h \,\mathrm{d}s \right| \leqslant \epsilon_h \|v_h\|_{L^1(e_h)}.$$

Proof. By the continuity of the functions v_h and $\jmath v_h$, Riemann and Lebesgue integration coincides. We show the assertion using the definition of Riemann integration. Let $\cup_i p_i$ be a partition of $\tilde{e}_h$. Then $\cup_i \phi_h^2(p_i)$ forms a partition of e_h. Since the map ϕ_h^2 is nonexpansive, the norm of the partition $\{\phi_h^2(p_i)\}$ tends to zero as that of $\{p_i\}$ goes to zero. For any choice of $\{x_i \in p_i\}$, there holds

$$\begin{aligned} \left| \int_{e_h} v_h \,\mathrm{d}s - \int_{\tilde{e}_h} \jmath v_h \,\mathrm{d}s \right| &= \lim_{n\to\infty} \left| \sum_i \left(v_h\big(\phi_h^2(x_i)\big) \big|\phi_h^2(p_i)\big| - \jmath v_h(x_i)|p_i| \right) \right| \\ &= \lim_{n\to\infty} \left| \sum_i v_h\big(\phi_h^2(x_i)\big) \big(\big|\phi_h^2(p_i)\big| - |p_i| \big) \right|. \end{aligned}$$

By part (ii) of lemma 4.2, there holds $||\phi_h^2(p_i)| - |p_i|| \leqslant \epsilon_h |\phi_h^2(p_i)|$, which concludes the proof. □

Remark 4.3. An inspection of the proof indicates that the lemma is valid for any function continuous over the domain $\overline{\Omega}_h$.

We shall also need a Riesz projection $\mathcal{R}_h$, which is dependent of the domain Ω_h.

Lemma 4.6. *Let the Riesz projection $\mathcal{R}_h : H^1(\Omega) \mapsto V_h$ be defined by*

$$\int_{\Omega_h} \nabla \mathcal{R}_h v \cdot \nabla v_h \,\mathrm{d}x + \int_{\Omega_h} \mathcal{R}_h v v_h \,\mathrm{d}x = \int_{\Omega_h} \nabla v \cdot \nabla v_h \,\mathrm{d}x + \int_{\Omega_h} v v_h \,\mathrm{d}x \quad \forall v_h \in V_h.$$

Then the operator $\mathcal{R}_h$ satisfies the following estimate

$$\lim_{h\to 0} \|\jmath \mathcal{R}_h v - v\|_{H^1(\Omega)} = 0 \quad \forall v \in H^1(\Omega).$$

Proof. Clearly, by the definition of the space $H^1(\Omega)$, there holds

$$\|\jmath \mathcal{R}_h v - v\|^2_{H^1(\Omega)} = \|\mathcal{R}_h v - v\|^2_{H^1(\Omega_h)} + \|\jmath \mathcal{R}_h v - v\|^2_{H^1(\Omega\setminus\Omega_h)}.$$

It suffices to estimate the two terms. We estimate the first term by a density argument. By Céa's lemma and the definition of Riesz projection, $\|\mathcal{R}_h v - v\|_{H^1(\Omega_h)} \leqslant \inf_{v_h \in V_h} \|v_h - v\|_{H^1(\Omega_h)}$. Then following [10, theorem 3.2.3] we deduce that for any $v \in C^\infty(\overline{\Omega})$, there holds

$$\|v - \mathcal{I}_h v\|_{H^1(\Omega_h)} \leqslant Ch|\Omega_h|^{\frac{1}{2}} \|v\|_{W^{2,\infty}(\Omega_h)},$$

where C does not depend on Ω_h. Now for any fixed $v \in H^1(\Omega)$, by the density of $C^\infty(\overline{\Omega})$ in $H^1(\Omega)$, there exists $v^\epsilon \in C^\infty(\overline{\Omega})$ with $\|v^\epsilon - v\|_{H^1(\Omega)} \leqslant \epsilon$ for any $\epsilon > 0$. Hence with the choice $v_h = \mathcal{I}_h v^\epsilon$ in Céa's lemma, there holds $\lim_{h\to 0} \|\mathcal{R}_h v - v\|_{H^1(\Omega_h)} = 0$. Meanwhile, by the triangle inequality we have

$$\begin{aligned} \|\jmath \mathcal{R}_h v - v\|_{H^1(\Omega\setminus\Omega_h)} &\leqslant \|\jmath \mathcal{R}_h v\|_{H^1(\Omega\setminus\Omega_h)} + \|v\|_{H^1(\Omega\setminus\Omega_h)} \\ &\leqslant C\epsilon_h^{\frac{1}{2}} \|\mathcal{R}_h v\|_{H^1(\Omega_h)} + \|v\|_{H^1(\Omega\setminus\Omega_h)} \to 0, \end{aligned}$$

where the last term tends to zero by Lebesgue dominated convergence theorem [15]. □

Next we establish an analogue of lemma 3.1 for the solution $(u_h, U_h) \in \mathbb{H}_h := H^1(\Omega_h) \otimes \mathbb{R}^L_\diamond$ to the discrete variational problem (on the polyhedral domain Ω_h):

$$\int_{\Omega_h} \sigma_h \nabla u_h \cdot \nabla v_h \,\mathrm{d}x + \sum_{l=1}^{L} z_l^{-1} \int_{e_{l,h}} (u_h - U_{h,l})(v_h - V_l)\,\mathrm{d}s = \sum_{l=1}^{L} I_l V_l, \quad \forall (v_h, V) \in \mathbb{H}_h. \tag{14}$$

There are several possible choices of the discrete surface $e_{h,l}$, which is a polyhedral approximation to the surface patch e_l (occupied by the electrode). A straightforward definition of $e_{h,l}$ would be $e_{l,h} = \phi_h(e_l)$. Here we let $e_{h,l} = \phi_h(\varrho_h(e_l))$. We note that in practice, the surface $e_{h,l}$ can be chosen to be the union of a collection of polyhedral surfaces only so as to avoid integration over a curved surface; and the analysis below remains valid for this case. Next we denote $\tilde{e}_{l,h} = \psi_h(e_{l,h}) \subset e_l$. By assumption 4.1(b), the measure $|e_l \backslash \tilde{e}_{l,h}|$ is bounded by $|\Gamma| - |\Gamma_h|$, with a limit zero as h goes to zero. By the Lax–Milgram theorem, for each fixed σ_h, there exists a unique solution $(u_h, U_h) \in \mathbb{H}_h$ to the discrete variational problem (14), and it satisfies the following *a priori* error estimate $\|(u_h, U_h)\|_{\mathbb{H}_h} \leqslant C\|I\|$. Hence by lemma 4.4, the sequence $\{(\jmath u_h, U_h)\}$ is uniformly bounded in $\mathbb{H}$ independent of h. Now we can state an important lemma on the convergence of the discrete forward map $\sigma_h \mapsto (\jmath u_h(\sigma_h), U_h(\sigma_h)) \in \mathbb{H}_h$.

Lemma 4.7. *Let $\{\sigma_h\} \subset \mathcal{A}$ and $(u_h(\sigma_h), U_h(\sigma_h))$ solve the discrete variational problem (14). If $\jmath\sigma_h$ converges to $\sigma \in \mathcal{A}$ in $L^1(\Omega)$, then the sequence $\{(\jmath u_h(\sigma_h), U_h(\sigma_h))\}$ converges to $(u(\sigma), U(\sigma))$ in $\mathbb{H}$.*

Proof. For simplicity, we denote the extensions of σ_h, u_h and v_h from Ω_h to Ω by $\tilde{\sigma}_h = \jmath\sigma_h$, $\tilde{u}_h = \jmath u_h(\sigma_h)$, $\tilde{v}_h = \jmath v_h$, and $\bar{u}_h = \jmath\mathcal{R}_h u$. Then the assumption $\sigma_h \in \mathcal{A}_h \subset V_h$, i.e., $c_0 \leqslant \sigma_h \leqslant c_1$, and *a priori* estimate for u_h, lemmas 4.4 and 4.3, imply that the sequence $\{\tilde{u}_h(\sigma_h)\}$ is uniformly bounded in $H^1(\Omega)$.

First we rewrite the discrete variational formulation (14) as

$$\begin{aligned}\int_\Omega \tilde{\sigma}_h \nabla\tilde{u}_h \cdot \nabla\tilde{v}_h \,\mathrm{d}x + \sum_{l=1}^{L} z_l^{-1} \int_{e_l} (\tilde{u}_h - U_{h,l})(\tilde{v}_h - V_l)\,\mathrm{d}s &= \int_{\Omega\backslash\Omega_h} \tilde{\sigma}_h \nabla\tilde{u}_h \cdot \nabla\tilde{v}_h \,\mathrm{d}x + \sum_{l=1}^{L} I_l V_l \\ &+ \sum_{l=1}^{L} z_l^{-1} \int_{e_l} (\tilde{u}_h - U_{h,l})(\tilde{v}_h - V_l)\,\mathrm{d}s \\ &- \sum_{l=1}^{L} z_l^{-1} \int_{e_{l,h}} (u_h - U_{h,l})(v_h - V_l)\,\mathrm{d}s, \quad \forall (v_h, V) \in \mathbb{H}_h\end{aligned}$$

and take the test function $(v_h, V) = (\mathcal{R}_h u - u_h, U - U_h)$. Next we subtract it from (2) with the test function $(v, V) = (\bar{u}_h - \tilde{u}_h, U - U_h)$ to get the identity for the error $(w, W) = (u - \bar{u}_h, U - U_h)$:

$$\begin{aligned}\int_\Omega \tilde{\sigma}_h |\nabla w|^2 \,\mathrm{d}x + \sum_{l=1}^{L} z_l^{-1} \int_{e_l} |w - W_l|^2 \,\mathrm{d}s &\leqslant \underbrace{\int_\Omega (\tilde{\sigma}_h - \sigma)\nabla u \cdot \nabla(\bar{u}_h - \tilde{u}_h)\,\mathrm{d}x}_{\mathrm{I}} \\ &+ \underbrace{\int_\Omega \tilde{\sigma}_h \nabla w \cdot \nabla(u - \bar{u}_h)\,\mathrm{d}x}_{\mathrm{II}} + \underbrace{\int_{\Omega\backslash\Omega_h} \tilde{\sigma}_h \nabla\tilde{u}_h \cdot \nabla(\bar{u}_h - \tilde{u}_h)\,\mathrm{d}x}_{\mathrm{III}} + \sum_{l=1}^{L} z_l^{-1} \underbrace{\int_{e_l} (w - W_l)(u - \bar{u}_h)\,\mathrm{d}s}_{\mathrm{IV}} \\ &+ \sum_{l=1}^{L} z_l^{-1} \underbrace{\left[\int_{e_l} (\tilde{u}_h - U_{h,l})((\bar{u}_h - \tilde{u}_h) - W_l)\,\mathrm{d}s - \int_{e_{l,h}} (u_h - U_{h,l})((\mathcal{R}_h u - u_h) - W_l)\,\mathrm{d}s\right]}_{\mathrm{V}}.\end{aligned}$$

Next we estimate the five terms (I–V) on the right-hand side. For the first term I, by the generalized Hölder's inequality we have

$$|\mathrm{I}| \leqslant \|\tilde{\sigma}_h - \sigma\|_{L^p(\Omega)} \|\nabla u\|_{L^q(\Omega)} \|\nabla(\bar{u}_h - \tilde{u}_h)\|_{L^2(\Omega)},$$

where the exponent q is from theorem 2.1, and the exponent $p > 0$ satisfies $\frac{1}{p} + \frac{1}{q} = \frac{1}{2}$. The factor $\|\nabla(\bar{u} - \tilde{u}_h)\|_{L^2(\Omega)}$ is uniformly bounded due to the bounds on u_h and $\mathcal{R}_h u$ and lemma 4.4. Meanwhile, there holds $\|\tilde{\sigma}_h - \sigma\|_{L^p(\Omega)} \leqslant C\|\tilde{\sigma}_h - \sigma\|_{L^1(\Omega)}^{\frac{1}{p}} \to 0$. Hence, the first term $\mathrm{I} \to 0$ as $h \to 0$. For the second term II, in view of lemma 4.6 and the uniform bound of the discrete admissible set $\mathcal{A}_h$, we have

$$|\mathrm{II}| \leqslant \|\tilde{\sigma}_h\|_{L^\infty(\Omega)} \|\nabla w\|_{L^2(\Omega)} \|\nabla(u - \bar{u}_h)\|_{L^2(\Omega)} \to 0.$$

Similarly, lemma 4.4 and uniform boundedness of $\|\nabla u_h\|_{L^2(\Omega)}$ and $\|\nabla(\mathcal{R}_h u - u_h)\|_{L^2(\Omega)}$ yield

$$\begin{aligned} |\mathrm{III}| &\leqslant C\|\tilde{\sigma}_h\|_{L^\infty(\Omega\setminus\Omega_h)} \|\nabla \tilde{u}_h\|_{L^2(\Omega\setminus\Omega_h)} \|\nabla(\bar{u}_h - \tilde{u}_h)\|_{L^2(\Omega\setminus\Omega_h)} \\ &\leqslant C\epsilon_h \|\nabla u_h\|_{L^2(\Omega_h)} \|\nabla(\mathcal{R}_h u - u_h)\|_{L^2(\Omega_h)} \to 0. \end{aligned}$$

Next we consider the boundary terms. By the trace theorem [15] and the approximation property of $\mathcal{R}_h$ in lemma 4.6, we get

$$|\mathrm{IV}| \leqslant \|w - W_l\|_{L^2(e_l)} \|u - \bar{u}_h\|_{L^2(e_l)} \leqslant C\|w - W_l\|_{L^2(e_l)} \|u - \bar{u}_h\|_{H^1(\Omega)} \to 0.$$

Lastly, for the term V, it suffices to consider the quantity $\int_{e_{l,h}} u_h v_h \,\mathrm{d}s - \int_{e_l} \tilde{u}_h \tilde{v}_h \,\mathrm{d}s$ with $v_h = \mathcal{R}_h u - u_h$, and the remaining terms can be bounded similarly. By letting $\tilde{e}_{l,h} = \psi_h(e_{l,h})$, the triangle inequality and lemma 4.5, we deduce that

$$\begin{aligned} \left| \int_{e_{l,h}} u_h v_h \,\mathrm{d}s - \int_{e_l} \tilde{u}_h \tilde{v}_h \,\mathrm{d}s \right| &\leqslant \left| \int_{e_{l,h}} u_h v_h \,\mathrm{d}s - \int_{\tilde{e}_{l,h}} \tilde{u}_h \tilde{v}_h \,\mathrm{d}s \right| + \left| \int_{e_l \setminus \tilde{e}_{l,h}} \tilde{u}_h \tilde{v}_h \,\mathrm{d}s \right| \\ &\leqslant \epsilon_h \|u_h v_h\|_{L^1(e_{l,h})} + \|\tilde{u}_h \tilde{v}_h\|_{L^1(e_l \setminus \tilde{e}_{l,h})} \\ &\leqslant \epsilon_h \|u_h v_h\|_{L^1(e_{l,h})} + \|\tilde{u}_h \tilde{v}_h\|_{L^1(e_l \setminus \tilde{e}_{l,h})} =: I_1 + I_2. \end{aligned}$$

It remains to bound the terms I_1 and I_2. By Sobolev embedding theorem [15] and uniform boundness of u_h in $H^1(\Omega_h)$, $\|u_h v_h\|_{L^1(e_{l,h})}$ is uniformly bounded for all h, hence $I_1 \to 0$ as $h \to 0$. By Sobolev embedding theorem, $H^1(\Omega)$ embeds continuously into $L^4(\Gamma)$ ($d = 2, 3$), and thus by Hölder's inequality, we deduce $\tilde{u}_h \tilde{v}_h \in L^2(\Gamma)$. Hence we can estimate the term I_2 by Hölder's inequality, the trace theorem and the uniform boundedness of $\tilde{u}_h$ and $\tilde{v}_h$ in $H^1(\Omega)$ as follows

$$\begin{aligned} I_2 &\leqslant \|\tilde{u}_h \tilde{v}_h\|_{L^2(e_l \setminus \tilde{e}_{l,h})} |e_l \setminus \tilde{e}_{l,h}|^{\frac{1}{2}} \\ &\leqslant \|\tilde{u}_h\|_{L^4(e_l)} \|\tilde{v}_h\|_{L^4(e_l)} |e_l \setminus \tilde{e}_{l,h}|^{\frac{1}{2}} \\ &\leqslant C\|\tilde{u}_h\|_{H^1(\Omega)} \|\tilde{v}_h\|_{H^1(\Omega)} |e_l \setminus \tilde{e}_{l,h}|^{\frac{1}{2}} \to 0. \end{aligned}$$

Now lemma 4.7 follows directly from the preceding estimates. □

Finally, we analyze the discrete optimization problem for curved domains:

$$\min_{\sigma_h \in \mathcal{A}_h} \left\{ J_h(\sigma_h) = \tfrac{1}{2}\|U_h(\sigma_h) - U^\delta\|^2 + \eta \Psi_h(\sigma_h) \right\}, \tag{15}$$

where the discrete approximation $U_h(\sigma_h)$ is defined by the finite element system (14), and the discrete penalty functional $\Psi_h(\sigma_h)$ is defined by

$$\Psi_h(\sigma_h) = \begin{cases} \frac{1}{2}\|\sigma_h\|_{H^1(\Omega_h)}^2, & \text{smoothness,} \\ |\sigma_h|_{\mathrm{TV}(\Omega_h)}, & \text{total variation.} \end{cases}$$

We observe that the penalty functional is defined only on the polyhedral approximation Ω_h, so the discrete optimization problem involves only computations on the approximate domain

Ω_h as well. Like before, the existence of a minimizer $\sigma_h^* \in \mathcal{A}_h$ to the discrete functional $J_h(\sigma_h)$ follows immediately from the compactness and norm equivalence in finite-dimensional spaces.

We now can show the convergence of the finite element approximation for curved domains.

Theorem 4.1. *Let assumption 4.1 be fulfilled and* $\{\sigma_h^*\}_{h>0}$ *be a sequence of minimizers to problem (15). Then the sequence* $\{\jmath\sigma_h^*\}_{h>0}$ *contains a convergent subsequence to a minimizer of problem (3) as the mesh size h tends to zero.*

(a) The convergence is weakly in $H^1(\Omega)$*, if* $\Psi_h(\sigma_h) = \frac{1}{2}\|\sigma_h\|^2_{H^1(\Omega_h)}$.
(b) The convergence is in $L^1(\Omega)$*, if* $\Psi_h(\sigma_h) = |\sigma_h|_{\mathrm{TV}(\Omega_h)}$.

Proof. We note that the constant function $\sigma_h = 1$ (with $\jmath\sigma_h = 1$) lies in the admissible set $\mathcal{A}_h$ for any h. Therefore, the sequence $\{\Psi_h(\sigma_h^*)\}$ is uniformly bounded. Next

$$\Psi(\jmath\sigma_h^*) - \Psi_h(\sigma_h^*) = \begin{cases} \frac{1}{2}\|\jmath\sigma_h^*\|^2_{H^1(\Omega\setminus\Omega_h)}, & \text{case (a)}, \\ |\jmath\sigma_h^*|_{\mathrm{TV}(\Omega\setminus\Omega_h)}, & \text{case (b)}. \end{cases}$$

Note that the function $\jmath\sigma_h^*$ is continuous and piecewise linear, and thus the bounded variation norm agrees with the $W^{1,1}(\Omega)$-norm. Hence we can apply lemma 4.4 to obtain

$$\limsup_{h\to 0} \Psi(\jmath\sigma_h^*) - \Psi_h(\sigma_h^*) = 0.$$

Hence the sequence $\{\Psi(\jmath\sigma_h^*)\}$ is also uniformly bounded, and by lemma 2.3, there exists a subsequence of $\{\jmath\sigma_h^*\}$ such that $\jmath\sigma_h^* \to \sigma^*$ in $L^1(\Omega)$. By lemma 4.7, we have $U_{l,h}(\sigma_h^*) \to U_l(\sigma^*)$ as $h \to 0$. This together with the weak lower semicontinuity of norms, we deduce that

$$\begin{aligned} J(\sigma^*) &= \tfrac{1}{2}\|U(\sigma^*) - U^\delta\|^2 + \alpha\Psi(\sigma^*) \\ &\leqslant \lim_{h\to 0} \tfrac{1}{2}\|U_h(\sigma_h^*) - U^\delta\|^2 + \alpha \liminf_{h\to 0} \Psi(\jmath\sigma_h^*) \\ &\leqslant \liminf_{h\to 0} \left(\tfrac{1}{2}\|U_h(\sigma_h^*) - U^\delta\|^2 + \alpha\Psi_h(\sigma_h^*) + \alpha(\Psi(\jmath\sigma_h^*) - \Psi_h(\sigma_h^*))\right) \\ &\leqslant \liminf_{h\to 0} J_h(\sigma_h^*) + \limsup_{h\to 0} \alpha(\Psi(\jmath\sigma_h^*) - \Psi_h(\sigma_h^*)) = \liminf_{h\to 0} J_h(\sigma_h^*), \end{aligned}$$

Now we proceed as in the proof of theorem 3.1 by considering cases (a) and (b) separately. For case (a), by the density of $C^\infty(\overline{\Omega})$ in $H^1(\Omega)$, we may assume $\sigma \in C^\infty(\overline{\Omega}) \cap \mathcal{A}$, then $\mathcal{I}_h\sigma \in \mathcal{A}_h$. Further,

$$\begin{aligned} \|\jmath\mathcal{I}_h\sigma - \sigma\|^2_{H^1(\Omega)} &= \|\jmath\mathcal{I}_h\sigma - \sigma\|^2_{H^1(\Omega_h)} + \|\jmath\mathcal{I}_h\sigma - \sigma\|^2_{H^1(\Omega\setminus\Omega_h)} \\ &\leqslant \|\mathcal{I}_h\sigma - \sigma\|^2_{H^1(\Omega_h)} + 2(\|\jmath\mathcal{I}_h\sigma\|^2_{H^1(\Omega\setminus\Omega_h)} + \|\sigma\|^2_{H^1(\Omega\setminus\Omega_h)}) \\ &\leqslant \|\mathcal{I}_h\sigma - \sigma\|^2_{H^1(\Omega_h)} + C\epsilon_h\|\mathcal{I}_h\sigma\|_{H^1(\Omega_h)} + 2\|\sigma\|^2_{H^1(\Omega\setminus\Omega_h)} \to 0. \end{aligned}$$

Then by lemma 4.7, $U_h(\mathcal{I}_h\sigma) \to U(\sigma)$ and thus $J(\sigma) = \lim_{h\to 0} J_h(\mathcal{I}_h\sigma) \geqslant \liminf_{h\to 0} J_h(\sigma_h^*) = J(\sigma^*)$, i.e., σ^* is a minimizer to the continuous functional.

Next consider case (b). For any fixed $\sigma \in \mathcal{A}$, by lemma 2.4 and the constructions in the proof of theorem 3.1, for any $\epsilon > 0$, there exists $\sigma^\epsilon \in C(\overline{\Omega})$ such that

$$\int_\Omega |\sigma^\epsilon - \sigma|\,\mathrm{d}x < \epsilon \quad \text{and} \quad \left|\int_\Omega |\nabla\sigma^\epsilon| - \int_\Omega |D\sigma|\right| < \epsilon.$$

Then $\tilde{\sigma}^\epsilon = P_{[c_0,c_1]}(\sigma^\epsilon) \in W^{1,\infty}(\Omega) \cap \mathcal{A}$. We take $\sigma_h = \mathcal{I}_h\tilde{\sigma}^\epsilon$. Then by lemma 4.4 there holds

$$\begin{aligned} \|\jmath\mathcal{I}_h\tilde{\sigma}^\epsilon - \tilde{\sigma}^\epsilon\|_{W^{1,1}(\Omega)} &= \|\jmath\mathcal{I}_h\tilde{\sigma}^\epsilon - \tilde{\sigma}\|_{W^{1,1}(\Omega_h)} + \|\jmath\mathcal{I}_h\tilde{\sigma}^\epsilon - \tilde{\sigma}^\epsilon\|_{W^{1,1}(\Omega\setminus\Omega_h)} \\ &\leqslant \|\mathcal{I}_h\tilde{\sigma}^\epsilon - \tilde{\sigma}^\epsilon\|_{W^{1,1}(\Omega_h)} + \|\jmath\mathcal{I}_h\tilde{\sigma}^\epsilon\|_{W^{1,1}(\Omega\setminus\Omega_h)} + \|\tilde{\sigma}^\epsilon\|_{W^{1,1}(\Omega\setminus\Omega_h)} \\ &\leqslant \|\mathcal{I}_h\tilde{\sigma}^\epsilon - \tilde{\sigma}^\epsilon\|_{W^{1,1}(\Omega_h)} + C\epsilon_h\|\mathcal{I}_h\tilde{\sigma}^\epsilon\|_{W^{1,1}(\Omega_h)} + \|\tilde{\sigma}^\epsilon\|_{W^{1,1}(\Omega\setminus\Omega_h)} \to 0. \end{aligned}$$

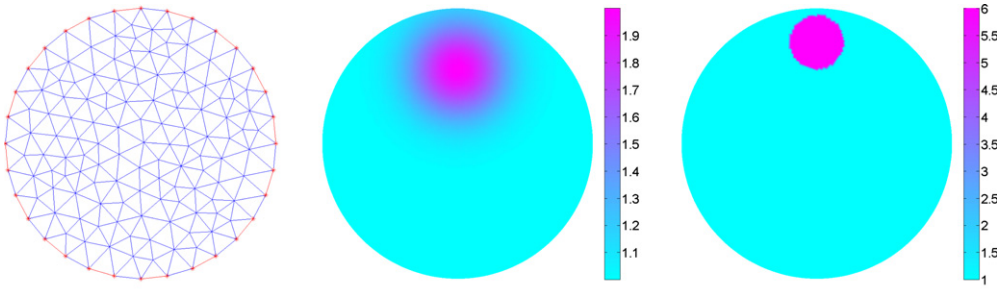

(a) domain and mesh (b) smooth $\sigma^\dagger$ (c) discontinuous $\sigma^\dagger$

Figure 1. (a) The domain Ω, and the coarse mesh (h_1), where the red lines denote the electrodes. (b), (c): the profile of the exact conductivity distribution $\sigma^\dagger$ for examples 1 and 2.

Then by lemma 4.7, $U_h(\mathcal{I}_h\tilde{\sigma}^\epsilon) \to U(\tilde{\sigma}^\epsilon)$ and thus $J(\tilde{\sigma}^\epsilon) = \lim_{h\to 0} J_h(\mathcal{I}_h\tilde{\sigma}^\epsilon) \geqslant \liminf_{h\to 0} J_h(\sigma_h^*) = J(\sigma^*)$. The rest is identical with the proof in theorem 3.1. This concludes the proof of the theorem. □

5. Numerical experiments

Now we present some numerical results to verify the convergence theory. The setup of the numerical experiments is as follows. The domain Ω is the unit disc centered at the origin, i.e., $\Omega = \{x = (x_1, x_2) : x_1^2 + x_2^2 < 1\}$. There are 16 electrodes $\{e_l\}_{l=1}^L$ uniformly distributed along the boundary Γ, each of the length $\pi/16$, thus occupying one half of the boundary Γ; see figure 1(a) for a schematic illustration of the domain and electrodes. The contact impedances $\{z_l\}_{l=1}^L$ on the electrodes $\{e_l\}_{l=1}^L$ are all set to unit, and the background conductivity σ_0 is taken to be $\sigma_0 \equiv 1$. For each experiment, we measure the electrode voltages U for five sinusoidal input currents. Then the noisy data U^δ is generated by adding componentwise Gaussian noise to the exact data $U(\sigma^\dagger)$ (with $\sigma^\dagger$ being the physical conductivity) as follows

$$U_i^\delta = U_i(\sigma^\dagger) + \epsilon \max_i |U_i(\sigma^\dagger)|\xi_i, \quad i = 1, \ldots, 16,$$

where ϵ is the noise level, and $\{\xi_i\}$ follow the standard normal distribution. We employ four quasi-uniform triangulations, with a mesh size of $h_1 = 1.27 \times 10^{-1}$, $h_2 = 6.37 \times 10^{-2}$, $h_3 = 3.18 \times 10^{-2}$ and $h_4 = 1.59 \times 10^{-2}$, respectively; see figure 1 for the coarsest mesh. The exact data $U(\sigma^\dagger)$ is computed on a much finer mesh, and the discrete minimizer $\sigma_{\alpha,h}^\delta$ on the finest mesh (with a mesh size h_4) is taken as the reference continuous minimizer σ_α^δ.

We consider the following two conductivity distributions.

Example 1. The true conductivity $\sigma^\dagger$ is given by $\sigma^\dagger(x) = \sigma_0(x) + \mathrm{e}^{-8(x_1^2+(x_2-0.55)^2)}$.

In this example, the true conductivity $\sigma^\dagger$ is a smooth blurb; see figure 1(b) for the profile. Hence, the $H^1(\Omega)$-smoothness penalty is suitable for the reconstruction. In table 1, we present the reconstruction error $e(h) = \|\sigma_{\alpha,h}^\delta - \sigma_\alpha^\delta\|_{L^2(\Omega)}$ for several different values of the regularization parameter α; see also figure 2 for exemplary reconstructions. Here the choice of α is not meant to be optimal, but only to study its influence on the convergence. The discrete Tikhonov minimizer $\sigma_{\alpha,h}^\delta$ was computed by a gradient descent algorithm. We observe that as the mesh size h decreases, the discrete minimizer $\sigma_{\alpha,h}^\delta$ converges to the reference one σ_α^δ. The convergence of the discrete minimizer $\sigma_{\alpha,h}^\delta$ tends to improve with the increase of the

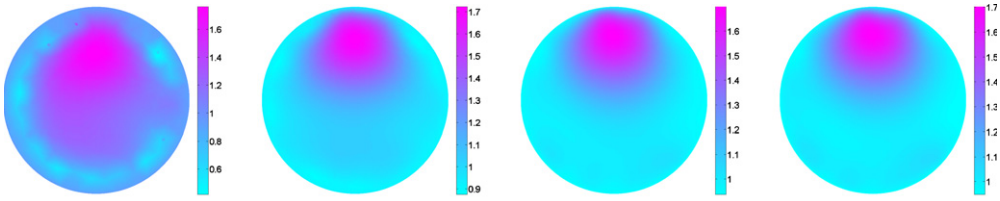

(a) $\sigma^{\delta}_{\alpha,h_1}$ (b) $\sigma^{\delta}_{\alpha,h_2}$ (c) $\sigma^{\delta}_{\alpha,h_3}$ (d) $\sigma^{\delta}_{\alpha,h_4}$

Figure 2. Reconstructions for example 1 with $\epsilon = 1 \times 10^{-3}$ and $\alpha = 5 \times 10^{-4}$.

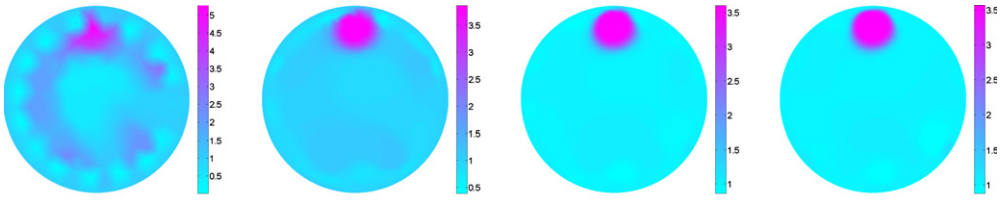

(a) $\sigma^{\delta}_{\alpha,h_1}$ (b) $\sigma^{\delta}_{\alpha,h_2}$ (c) $\sigma^{\delta}_{\alpha,h_3}$ (d) $\sigma^{\delta}_{\alpha,h_4}$

Figure 3. Reconstructions for example 2 with $\epsilon = 1 \times 10^{-3}$ and $\alpha = 5 \times 10^{-4}$.

Table 1. Numerical results for example 1.

ϵ	α	$e(h_1)$	$e(h_2)$	$e(h_3)$
0	1×10^{-4}	4.02×10^{-1}	1.14×10^{-1}	2.78×10^{-2}
1×10^{-3}	5×10^{-4}	3.71×10^{-1}	9.59×10^{-2}	2.43×10^{-2}
1×10^{-3}	1×10^{-3}	3.32×10^{-1}	8.78×10^{-2}	2.56×10^{-2}
1×10^{-3}	5×10^{-3}	2.91×10^{-1}	7.18×10^{-2}	1.74×10^{-2}

Table 2. Numerical results for example 2.

ϵ	α	$e(h_1)$	$e(h_2)$	$e(h_3)$
0	1×10^{-4}	1.04×10	3.73×10^{-1}	7.82×10^{-2}
1×10^{-3}	1×10^{-4}	1.05×10	3.47×10^{-1}	1.08×10^{-1}
1×10^{-3}	5×10^{-4}	1.03×10	2.53×10^{-1}	7.40×10^{-2}
1×10^{-3}	1×10^{-3}	9.98×10^{-1}	2.37×10^{-1}	6.27×10^{-2}

parameter α. This might be attributed to the fact that the larger is the α value, the more stable is the Tikhonov functional $J_{\alpha,h}(\sigma_h)$, and thus the discrete minimizer $\sigma^{\delta}_{\alpha,h}$ is less sensitive to the discretization error. However, a complete theoretical justification of this observation is still missing. Further, the reconstructions in figure 2 indicate that for the coarse meshes, the discretization error may cause fairly pronounced errors, as evidenced by spurious oscillations around the boundary Γ.

Example 2. The true conductivity $\sigma^{\dagger}$ is given by $\sigma^{\dagger} = \sigma_0 + 5\chi_S$, where χ_S denotes the characteristic function of the circle $S = \{(x_1, x_2) \in \mathbb{R}^2 : x_1^2 + (x_2 - 3/4)^2 \leqslant 0.04\}$.

Here the true conductivity $\sigma^{\dagger}$ is piecewise constant, cf figure 1(c) for the profile. Hence, the total variation seminorm regularization is suitable. The numerical results are presented in table 2; see also figure 3 for some reconstructions. The discrete Tikhonov minimizer $\sigma^{\delta}_{\alpha,h}$

was computed by an iteratively reweighted least-squares method [11]. The observations from example 1 remain valid: the discrete minimizer $\sigma_{\alpha,h}^{\delta}$ converges to the reference solution as the mesh size h decreases, and the convergence is better for larger regularization parameters. In contrast to the smoothness penalty, the total variation reconstruction is always piecewise constant: even the part away from the boundary is very sharply resolved, and the support estimate of the true conductivity is very satisfactory.

6. Concluding remarks

We have provided a convergence analysis of finite element approximations of the electrical impedance tomography with the popular complete electrode model. We investigated regularization formulations of Tikhonov type with either the smoothness or total variation penalty, which represent the two most popular imaging algorithms in practice. The convergence of the minimizers to the discrete Tikhonov functional for both polyhedral and convex smooth curved domains was established. The case of curved domains relies crucially on a careful analysis of the errors incurred by the domain approximation. This provides partial theoretical justifications of the so-far ad hoc discretization strategy. Our numerical experiments fully confirmed the convergence theory.

There are several avenues for further investigation. One immediate future problem is the convergence rates analysis, i.e., the error between the (discrete) approximation and the true solution in terms of the noise level and mesh size. This would shed valuable insights into the practically very important question of designing discretization strategies compatible with the regularization parameter and noise level so as to effect optimal computational complexity. The second is the development and analysis of an adaptive discretization strategy. This is motivated by the following observations: for the EIT inverse problem, the conductivity may have discontinuities, e.g., that by the total variation regularization, and thus the forward solution has limited global regularity. Further, the 'mixed-type' boundary condition in the complete electrode model causes inherent weak singularity around the electrodes. To efficiently and accurately resolve such singularities in the forward solution, an adaptive strategy is highly desirable.

Acknowledgments

The work of the second author (BJ) was partially supported by NSF grant DMS-1319052, and that of the third author (XL) was supported by National Science Foundation of China 11101316 and 91230108.

References

[1] Adler A, Gaburro R and Lionheart W 2011 Electrical impedance tomography *Handbook of Mathematical Methods in Imaging* ed O Scherzer (Berlin: Springer)
[2] Attouch H, Buttazzo G and Michaille G 2006 *Variational Analysis in Sobolev and BV Spaces* (Philadelphia: SIAM)
[3] Bernardi C 1989 Optimal finite element interpolation on curved domains *SIAM J. Numer. Anal.* **26** 1212–40
[4] Borcea L 2002 Electrical impedance tomography *Inverse Problems* **18** R99–R136
[5] Borsic A, Graham B M, Adler A and Lionheart W R B 2010 *In vivo* impedance imaging with total variation regularization *IEEE Trans. Med. Imaging* **29** 44–54
[6] Bramble J H and King J T 1994 A robust finite element method for nonhomogeneous Dirichlet problems in domains with curved boundaries *Math. Comput.* **63** 1–17

[7] Chen Z and Zou J 1999 An augmented Lagrangian method for identifying discontinuous parameters in elliptic systems *SIAM J. Control Optim.* **37** 892–910
[8] Cheng K-S, Isaacson D, Newell J C and Gisser D G 1989 Electrode models for electric current computed tomography *IEEE Trans. Biomed. Eng.* **36** 918–24
[9] Chung E T, Chan T F and Tai X-C 2005 Electrical impedance tomography using level set representation and total variational regularization *J. Comput. Phys.* **205** 357–72
[10] Ciarlet P G 2002 *The Finite Element Method for Elliptic Problems* (Philadelphia: SIAM)
[11] Clason C, Jin B and Kunisch K 2010 A semismooth Newton method for L^1 data fitting with automatic choice of regularization parameters and noise calibration *SIAM J. Imaging Sci.* **3** 199–231
[12] Dobson D C and Santosa F 1994 An image-enhancement technique for electrical impedance tomography *Inverse Problems* **10** 317–34
[13] Engl H, Kunisch K and Neubauer A 1989 Convergence rates for Tikhonov regularisation of nonlinear ill-posed problems *Inverse Problems* **5** 523–40
[14] Ervedoza S and de Gournay F 2011 Uniform stability estimates for the discrete Calderón problems *Inverse Problems* **27** 125012
[15] Evans L C and Gariepy R F 1992 *Measure Theory and Fine Properties of Functions* (Boca Raton, FL: CRC Press)
[16] Fichtenholz G M 2003 *Foundations of Mathematical Analysis* vol 3 (Moscow: Fizmatlit Publishers)
[17] Gallouet T and Monier A 2000 On the regularity of solutions to elliptic equations *Rend. Mat. Appl.* **19** 471–88
[18] Gehre M, Kluth T, Lipponen A, Jin B, Seppänen A, Kaipio J P and Maass P 2012 Sparsity reconstruction in electrical impedance tomography: an experimental evaluation *J. Comput. Appl. Math.* **236** 2126–36
[19] Gröger K 1989 A $W^{1,p}$-estimate for solutions to mixed boundary value problems for second order elliptic differential equations *Math. Ann.* **283** 679–87
[20] Harrach B and Seo J K 2010 Exact shape-reconstruction by one-step linearization in electrical impedance tomography *SIAM J. Math. Anal.* **42** 1505–18
[21] Jin B, Khan T and Maass P 2012 A reconstruction algorithm for electrical impedance tomography based on sparsity regularization *Int. J. Numer. Methods Eng.* **89** 337–53
[22] Jin B and Maass P 2012 An analysis of electrical impedance tomography with applications to Tikhonov regularization *ESAIM: Control Optim. Calc. Var.* **18** 1027–48
[23] Jin B and Maass P 2012 Sparsity regularization for parameter identification problems *Inverse Problems* **28** 123001
[24] Kaipio J P, Kolehmainen V, Somersalo E and Vauhkonen M 2000 Statistical inversion and Monte Carlo sampling methods in electrical impedance tomography *Inverse Problems* **16** 1487–522
[25] Karhunen K, Seppänen A, Lehikoinen A, Monteiro P J and Kaipio J P 2010 Electrical resistance tomography imaging of concrete *Cement Concr. Res.* **40** 137–45
[26] Knudsen K, Lassas M, Mueller J L and Siltanen S 2009 Regularized D-bar method for the inverse conductivity problem *Inverse Problems Imaging* **3** 599–624
[27] Kolehmainen V, Lassas M and Ola P 2005 The inverse conductivity problem with an imperfectly known boundary *SIAM J. Appl. Math.* **66** 365–83
[28] Lechleiter A and Rieder A 2006 Newton regularizations for impedance tomography: a numerical study *Inverse Problems* **22** 1967–87
[29] Lechleiter A and Rieder A 2008 Newton regularizations for impedance tomography: convergence by local injectivity *Inverse Problems* **24** 065009
[30] Lukaschewitsch M, Maass P and Pidcock M 2003 Tikhonov regularization for electrical impedance tomography on unbounded domains *Inverse Problems* **19** 585–610
[31] Meyers N G 1963 An L^p-estimate for the gradient of solutions of second order elliptic divergence equations *Ann. Scuola Norm. Sup. Pisa* **17** 189–206
[32] Rondi L 2008 On the regularization of the inverse conductivity problem with discontinuous conductivities *Inverse Problems Imaging* **2** 397–409
[33] Rondi L and Santosa F 2001 Enhanced electrical impedance tomography via the Mumford-Shah functional *ESAIM Control Optim. Calc. Var.* **6** 517–38
[34] Siltanen S, Mueller J and Isaacson D 2000 An implementation of the reconstruction algorithm of A Nachman for the 2D inverse conductivity problem *Inverse Problems* **16** 681–99

[35] Somersalo E, Cheney M and Isaacson D 1992 Existence and uniqueness for electrode models for electric current computed tomography *SIAM J. Appl. Math.* **52** 1023–40

[36] Vauhkonen M, Vadász D, Karjalainen P A, Somersalo E J and Kaipio J P 1998 Tikhonov regularization and prior information in electrical impedance tomography *IEEE Trans. Med. Imaging* **17** 285–93

[37] Vauhkonen P J, Vauhkonen M, Savolainen T and Kaipio J P 1999 Three-dimensional electrical impedance tomography based on the complete electrode model *IEEE Trans. Biomed. Eng.* **46** 1150–60